Journal of Structural Geology, Vol. 13, No. 10, pp. 1137 to 1156, 1991
Printed in Great Britain

0191-8141/91 $03.00+0.00

Fluid-enhanced deformation: transformation of granitoids to banded mylonites, western Sierra Nevada, California, and southeastern Australia

OTHMAR T. TOBISCH

Earth Science Board, University of California, Santa Cruz, CA 95064, U.S.A.

MARK D. BARTON*

Department of Earth and Space Sciences, University of California, Los Angeles, CA 90024-1567, U.S.A.

RON H. VERNON

School of Earth Sciences, Macquarie University, Sydney, NSW 2109, Australia

and

SCOTT R. PATERSON

Department of Geological Sciences, University of Southern California, Los Angeles, CA 90089-0740, U.S.A.

(*Received* 3 *September* 1990; *accepted in revised form* 2 *May* 1991)

Abstract—Deformation of tonalite and adamellite from the western Sierra Nevada, California, and southeastern Australia has produced mylonite zones that show a broad range of microstructural development, varying from strongly banded and/or foliated to locally non-foliated. Accompanying these fabrics are new mineral assemblages, commonly rich in quartz and epidote. Whereas the banded foliated varieties appear to develop from progressive deformation of the granitic host, they also occur in close proximity (cm–m) to domains of non-banded and/or weakly to non-foliated fabrics of similar mineralogy, suggesting a complex timing and partitioning of deformation, fluid flow and metamorphism in the mylonite zone.

Whole-rock major and trace element analyses of the tonalites show large enrichments of SiO_2, CaO, Fe_2O_3, total Fe and Sr, and strong depletions in Na_2O, K_2O, FeO, MgO, Ba and Rb with increasing stages of deformation, although substantial chemical change appears to occur under static conditions locally. Chemical changes in the adamellite are much less dramatic. All suites show systematic decrease in $\delta^{18}O$ and convergence of oxygen isotopic compositions of whole-rock and quartz with increasing deformation. *Minimum* fluid/rock is estimated to lie between 0.1 and 10, increasing with intensity of deformation and depending on host composition. Isotopically exchanged seawater or connate water are the most plausible fluids.

Chemical data from a number of mylonite zones in various orogenic belts show widely varying behavior (gain/loss) of major and minor elements. Eleven factors control which (and how much) elements are gained/lost during mylonitization of the granitoids, the most influential of which are primary composition, mineralogy and primary texture of the host, as well as several aspects of fluid interaction active during deformation. These influences may be a function of local rather than regional geological conditions.

INTRODUCTION

THE nature, geometry and mechanisms of formation of microstructures formed during mylonitization of granitoids are well-known from field and model/experimental studies (e.g. Ramsay & Graham 1970, Burg & Laurent 1977, Mitra 1978, Berthé *et al.* 1979, Vernon *et al.* 1983, Tullis & Yund 1985, 1987, Passchier & Simpson 1986, Simpson 1986, Hanmer 1987). Although geologists are becoming increasingly aware of the importance of fluid flow and fluid–rock interaction during metamorphic processes in general (e.g. Fyfe *et al.* 1978, Etheridge *et al.* 1983, 1984, Ferry 1986), the variations in chemical changes that may take place during mylonitization of granitoids are not well understood. Work done to date shows that during deformation, granitoids may behave essentially isochemically (e.g. Kerrich *et al.* 1980) or undergo moderate to large gain and/or loss of major and minor elements (e.g. Beach 1976, Sinha *et al.* 1986, Dipple *et al.* 1990)

The present study focuses on deformation of granitoids in which the timing relations between deformation, metamorphic–chemical changes and fluid flow are complex. Figure 1 illustrates some of the possible sequences that might arise over time in a zone of ductile shear:

(a) fracture formation → fluid flow along fracture with formation of a new mineral assemblage → ductile shear of new mineral assemblage not accompanied by further fluid flow;

(b) fracture formation → ductile shearing → fluids using ductile shear zone as conduit and produce new assemblages with static textures;

(c) fracture formation → synchronous occurrence of fluid flow (initially along fractures), new mineral assemblages and ductile shearing;

*Present address: Department of Geosciences, University of Arizona, Tuscon, AZ 85721, U.S.A.

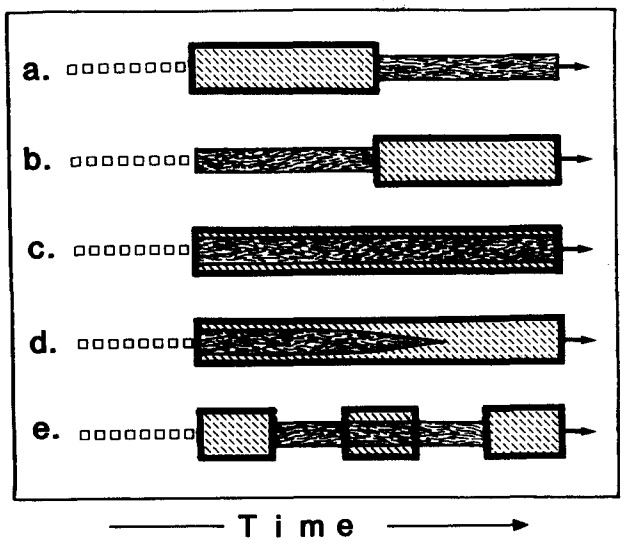

Fig. 1. Hypothetical models of structural sequences representing various combinations of *fracture formation* (line of small squares), *ductile deformation* (anastomosing wavy line pattern framed by thin lines) and *fluid flow* accompanied by neocrystallization and recrystallization (slanted dashes framed by thick lined box). See text for details.

(d) same as (c) but fluid flow continues along (parts of) the ductile shear zone after deformation ceases, producing domains where new mineral assemblages form with static textures;

(e) cyclic or irregular repetition of some combination of (a)–(d).

In addition to the above sequential processes, partitioning of deformation and variations in fluid flow path could produce new mineral assemblages resulting in a complex three-dimensional array of overlapping zones. In such a situation, it would be difficult to document whether chemical changes occurring in a ductile shear zone are strictly synkinematic or result from a complex history (e.g. Fig. 1e).

In the rocks discussed herein, tonalite is observed to grade into banded mylonite bearing mineral assemblages atypical of shear zones described in the literature (e.g. Sinha *et al.* 1986). In the tonalites, grain size reduction may be only moderate, but chemical and mineralogical changes are commonly extreme, indicating that substantial removal and addition of material has occurred, and that fluids have played an important role in the generation of the mylonites.

In the following pages, we describe microstructural changes associated with the deformation of two tonalites and a biotite adamellite, and discuss the resulting geochemical changes. We then compare our results with chemical studies on other granitoid mylonites.

GEOLOGICAL FRAMEWORK

Mylonites in tonalitic plutons from the Foothills Terrane, west-central Sierra Nevada, California, and from the Lachlan Fold Belt, southeastern Australia, show remarkably similar microstructural and chemical changes, but differ from those in a biotite adamellite in the Lachlan Fold Belt. The geometry of meso- and microscopic fabrics, as well as regional considerations, indicate that all three plutons are cut by zones of ductile deformation, but that the kinematic patterns during mylonitization were different. In the Foothills Terrane tonalite, the fabrics show a strong resemblance to those generated by bulk heterogeneous flattening (e.g. Choukroune & Gapais 1983; cf. also Tobisch *et al.* 1989), whereas the Lachlan Fold Belt plutons are characterized either by thrusting (Tobisch & Paterson 1990) or strike-slip movement (Vernon *et al.* 1983, and unpublished data).

We will now describe the regional setting of the study areas, and then consider the textural and chemical development of the mylonites.

Regional settings

Foothills Terrane, western Sierra Nevada. In the Foothills Terrane (Fig. 2), several late Jurassic tonalitic to gabbroic plutons have intruded volcanic-arc and pelitic rocks of mid-Jurassic age (Clark 1964). The wall rocks and some of the granitoids have undergone multiple deformations and greenschist to lower amphibolite facies dynamothermal metamorphism (Tobisch *et al.* 1989). The pluton under consideration is a hornblende tonalite, called the Santa Cruz Mountain tonalite (SCMT), which was emplaced prior to ductile deformation in the wall rocks. The Bear Mountains fault zone (Clark 1964, Paterson *et al.* 1987), a zone of ductile strain that attains a maximum width of *ca* 7 km, is the locus of more complex ductile deformation and elevated metamorphism than surrounding rocks (Fig. 2). Local development of high-temperature (upper amphibolite to granulite facies) mylonite has been documented within part of this fault zone (Vernon *et al.* 1989).

West of the Bear Mountains fault is a parallel zone of very strong deformation. The rocks in this zone have anastomosing planar fabrics varying in morphology between strongly foliated, mylonitic and banded mylonitic, and occur in a zone about 2–2.5 km wide within the SCMT and within hornblende diorite/gabbro (hd/g) intruded into wall rock immediately to the southeast (Fig. 2; hd/g not shown). However, the mylonites lose their identity in the strongly foliated wall rock about 2–4 km beyond the pluton.

The mylonite zone lies on the boundary between biotite zone (greenschist facies) and lower amphibolite facies rocks (cf. Fig. 2 and Tobisch *et al.* 1989, fig 6), and is characterized by varying amounts of chlorite and epidote. The mylonitization is interpreted as a zone of retrogressive metamorphism accompanied by intense deformation. The abrupt gradient between the chlorite-bearing and amphibolite facies assemblages, the apparent narrowing (and eventual attenuation) of the mylonitic fabrics and their chlorite-bearing assemblages along strike from the pluton, as well as abundant thin section and chemical data presented below, suggest that the localized deformation and new mineral assemblages represent a fluid-enhanced (controlled?) phenomenon.

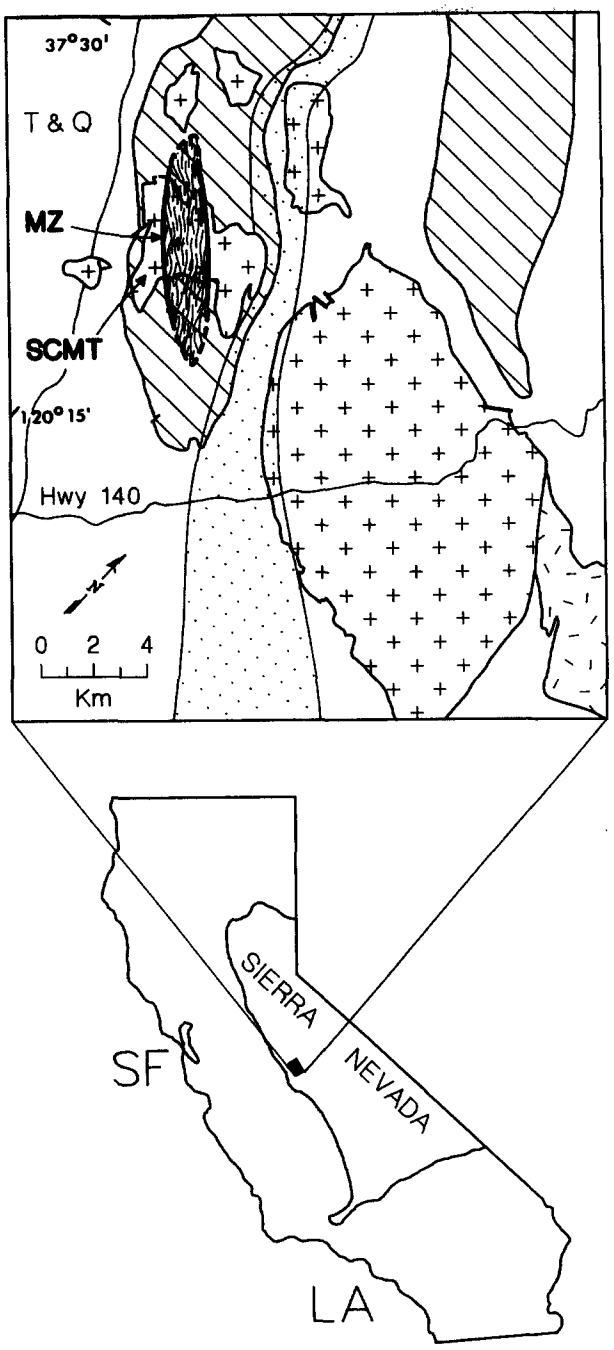

Fig. 2. Locality map of the study area in the Foothills Terrane of the central Sierra Nevada, California. Diagonal lines = volcanic rocks of late Triassic (northern outcropping on map) to late Jurassic age; no pattern = slate, sandstone and associated sedimentary rocks of late Jurassic age; crosses = plutonic rocks of late Jurassic age; random line pattern = plutonic rocks of early Cretaceous age; stippled zone = zone of intense repeated deformation (Bear Mountains fault zone); anastomosing wavy-line pattern = mylonite zone (MZ) discussed in text; thick lines = faults and shear zone boundary; T & Q = Tertiary and Quaternary deposits; SCMT = Santa Cruz Mountain tonalite; SF = San Francisco; LA = Los Angeles. Regional trend of foliation and bedding is northwest, approximately parallel to the Bear Mountains fault zone (see Tobisch *et al.* 1989 for further details).

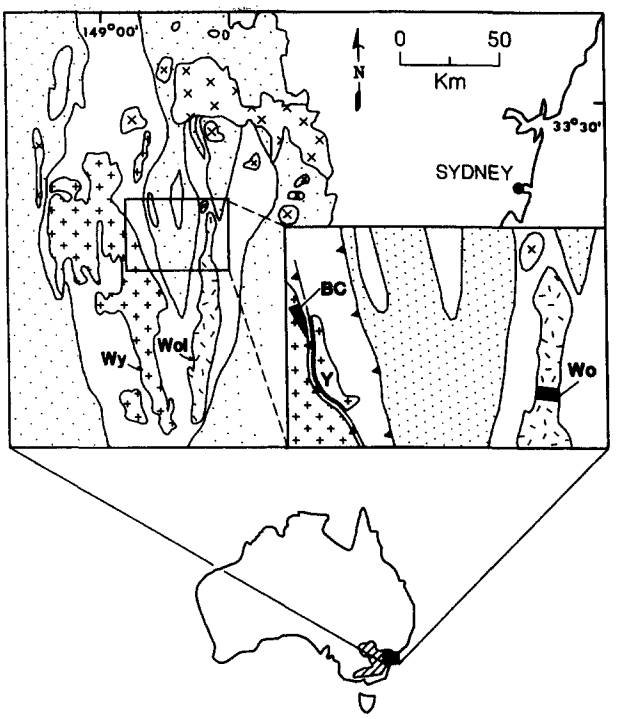

Fig. 3. Map showing locality of the Lachlan Fold Belt in southeastern Australia (lower diagram). Upper diagram shows simplified geology of the eastern part of that Fold Belt, with special reference to parts of the Wyangala Batholith (**Wy**; crosses) and the Wologorong Batholith (**Wol**; random lines) enclosed within box. Stippled area = predominantly Silurian and Devonian sedimentary and volcanic rocks; no pattern = predominantly Ordovician sedimentary rocks; crosses = Bathurst Batholith and related plutons; no pattern in eastern part of main figure around Sydney = predominantly sedimentary rocks of Permo-Triassic age. Inset: blow-up box showing detail of studied areas in those two batholiths. Lines with barbs = thrusts or ductile shear zones, barbed side on upper plate; **BC** = Blackman's Creek tonalite; **Wo** = area along Abercrombie River where samples were taken from the Wologorong Batholith; **Y** = Yarra granite (see Tobisch & Paterson 1990, fig. 3, for further details).

Lachlan Fold Belt, southeastern Australia. The Lachlan Fold Belt is characterized by large elongate mid-Paleozoic batholiths that have intruded into lower Paleozoic sedimentary and volcanic rocks (Cas 1983, Chappell *et al.* 1988). One such composite body is the Wyangala Batholith (Fig. 3), which is made up of both I- and S-type granitoids (White 1983). A leucogranite mapped along the northeastern edge of the batholith by Gibson (1973) contains a tonalitic phase known as the Blackman's Creek tonalite (BCT), which outcrops over a relatively small area (BC, Fig. 3, inset). Detailed geologic mapping in this area by Tobisch & Paterson (1990, fig. 3) indicates that the BCT, like the leucogranite, lies on the edge of a zone of ductile thrusting. Structural relations indicate that the leucogranite/BCT was emplaced penecontemporaneously with the thrusting under greenschist facies (biotite zone) conditions (Tobisch & Paterson 1990).

Further to the east, a highly elongate composite granitoid known as the Wologorong Batholith crops out (Wol, Fig. 3), and is separated from the Wyangala Batholith (and BCT) by thrusts (Hobbs 1965, Paterson *et al.* 1990). Although some parts of the Wologorong batholith are virtually structureless, many regions are characterized by well-developed solid-state *S–C* folia and thin zones of ultramylonite (Vernon *et al.* 1983). Mineral assemblages indicate the rocks were deformed under conditions of the greenschist facies (biotite zone).

Outcrop characteristics of deformed SMCT and BCT

Deformation in these tonalites is generally strong, and a well-developed pervasive foliation occurs in most exposures. Locally, highly stretched fabrics ($L > S$) predominate. The partitioning of strain is most heterogeneous in the SCMT, portions of which show a nearly complete range in deformation from weakly foliated to banded mylonitic fabrics (Fig. 4). The weakly foliated parts of the SCMT preserve earlier stages of fabric development, allowing us to evaluate the genesis of the more strongly deformed parts of the tonalites. Below, we outline the main features of deformation that are common to the tonalites in both areas, referring to the specific areas where appropriate.

In the less pervasively deformed parts of the pluton, incipient stages of mylonitization can be seen along fractures, which are orientated at high angles to each other (Fig. 4a). Mineral assemblages in these narrow (usually 2–3 cm) zones of deformation are dominated by quartz–chlorite–epidote. With increasing foliation development, these zones become orientated at smaller angles to each other, and deformation along them is wider, forming a network of anastomosing mylonite zones (Fig. 4b). Where the foliation in the tonalite is strongest, the mylonite zones are orientated largely parallel to the foliation in the tonalite, and heterogeneously banded mylonite zones, commonly >1 m in width, occur (Tobisch *et al.* 1989, fig. 4b). In the BCT, deformation appears to be more homogeneous than in the SCMT. Most outcrops of BCT show a strong foliation and lineation; banded mylonite zones are less common, and where present, they occur parallel to the foliation (Fig. 5a).

Microstructural development of the mylonites

In the least deformed and metamorphosed samples, the tonalites consist of primary green to blue-green hornblende and zoned plagioclase, with recrystallized quartz and varying amounts of metamorphic chlorite, epidote, actinolite/hornblende, opaque grains and other minor minerals (Figs. 5b and 6a). In some thin sections, longitudinally twinned plagioclase laths show alignment of their long axes, suggesting that the foliation may have a component of magmatic flow (Paterson *et al.* 1989). However, the major part of the fabric developed in the solid-state. With increasing deformation and recrystallization, these foliated tonalites undergo grain size reduction. The change in grainsize of quartz in the SCMT commonly is greater than one order of magnitude (2–0.08 mm), and in some localized domains, two orders of magnitude. Although the original grain size of the BCT is unknown because of pervasive deformation, available samples contain quartz that changes by at least an order of magnitude (4–0.1 mm). Kinematic indicators in the BCT support eastward-directed thrusting, as outlined by Tobisch & Paterson (1990), whereas those observed in the SCMT are ambiguous and their regional significance requires further study.

Some of the textural–mineralogical changes that occur with increasing fabric development are as follows (Figs. 5 and 6).

(1) Igneous plagioclase fractures and forms angular fragments, shows bent or faulted twins, and may be replaced in part by epidote (Figs. 5b and 6a & b), altered to white mica, or be removed by dissolution. Microprobe analysis (carried out by RHV at Macquarie University on an ETEC Autoprobe with automated LINK energy dispersive system) of plagioclase in the SCMT suite indicates a composition of An_{27}–An_{53} values one expects to find in epidote amphibolite and higher grade rocks (Miyashiro 1973), and they probably reflect original igneous compositions.

(2) Hornblende fractures into smaller fragments and/or is altered in varying degrees to chlorite (biotite in the BCT), epidote, and/or metamorphic amphibole (± opaque minerals–mt?), and commonly is replaced by those metamorphic minerals (Figs. 5b and 6a). Microprobe analysis of igneous and metamorphic amphibole indicate their compositions are comparable; average Mg/Mg + Fe + Mn ratios mostly fall in the range 56–59 (46.7 min–65.4 max), with a tendency for X_{Mg} to increase with deformation intensity; compositions are unusually edenitic, resembling calcic amphiboles from low-pressure metamorphic terranes (Robinson *et al.* 1982).

(3) Plagioclase and hornblende of igneous parentage disappear from the rock at about the same intensity of fabric development (Fig. 7).

(4) Quartz decreases in grainsize and increases in mode in the strongly mylonitic (SCMT-3,4) and banded rocks (SCMT-2 and BC-42A; Fig. 7). It occurs in progressively more elongate aggregates of neoblasts, which show a tendency for individual grains to be elongate parallel (or locally at a small angle) to the foliation (Fig. 6b). Undulatory extinction and subgrain formation is common, and ribbon quartz occurs in some samples.

(5) Epidote occurs with increasingly greater volume with fabric development (Fig. 7), both in the matrix, in microveins, and replacing plagioclase. It commonly has undulatory extinction. Microprobe analysis of epidote and chlorite in the SCMT suite indicates that with increasing deformation, epidote tends to become richer in the clinozoisite component (X_{Ps} = 0.85–0.55), and chlorite becomes slightly more magnesian (Mg/Mg + Fe + Mn = 0.58–0.63). In addition, zoning in epidote has been observed in back-scattered electron images in one sample of banded quartz–epidote mylonite from the SCMT, and X-ray mapping of the epidote indicates the zoning is largely due to variations in Fe^{3+} (S. Sorensen personal communication, 1990), indicating that compositional changes took place during epidote growth.

(6) The tonalite is eventually transformed into a quartz–epidote rock occurring in two general geometries, *banded* and *non-banded*:

(a) *banded mylonite* is characterized by layers of quartz–epidote with minor (i.e. 1–2%) chlorite and/or actinolite, which alternate with bands of nearly pure

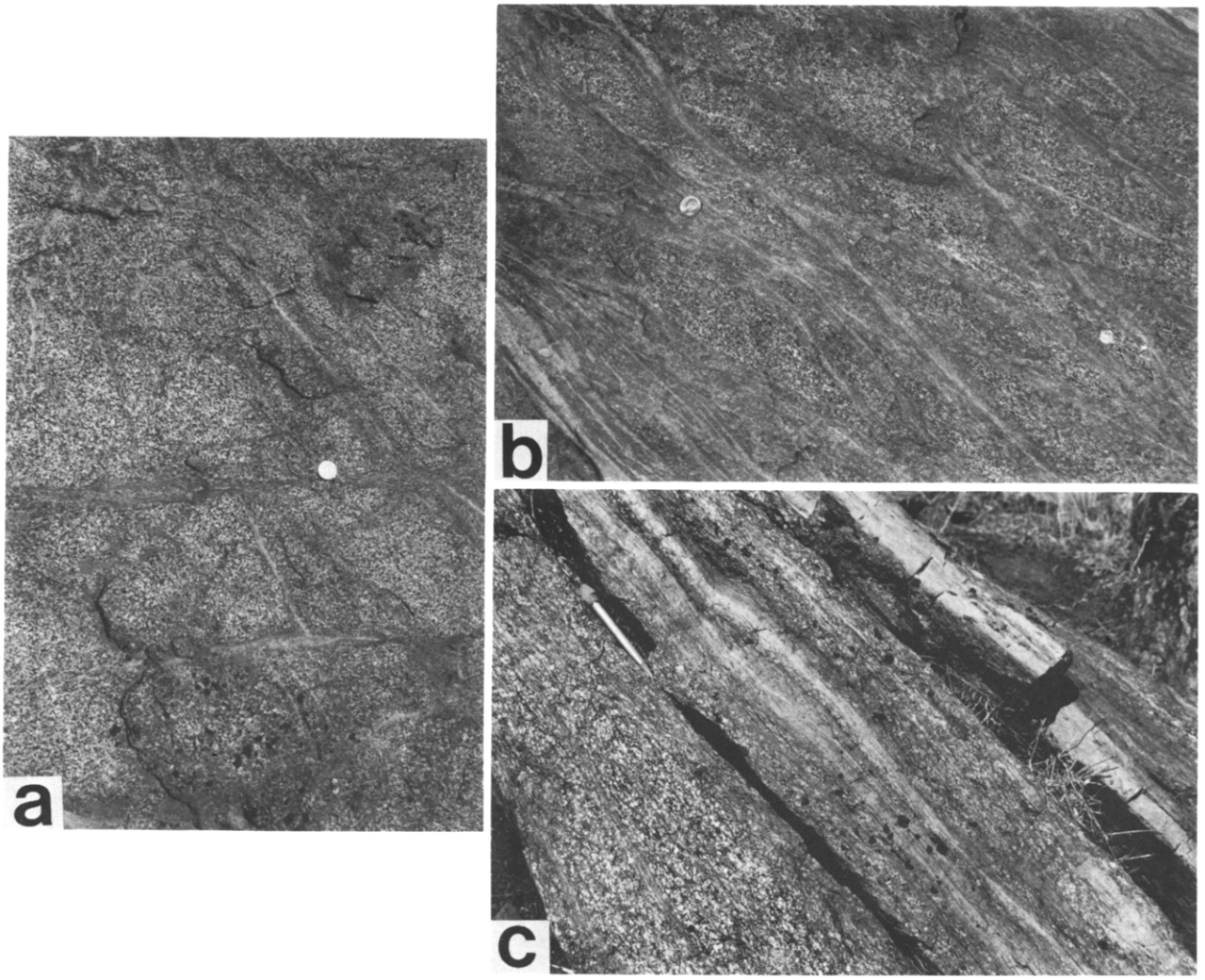

Fig. 4. Field photographs of the Santa Cruz Mountain tonalite (SCMT) in various stages of mylonitization. Photographs taken in central part of the mylonite zone about half way between northern and southern pluton contacts, Fig. 2. (a) Fractures inclined at relatively high angles along which alteration and some deformation has taken place; host tonalite weakly foliated. Coin is 2.3 cm in diameter. (b) Fractures inclined at a smaller angle, showing alteration and deformation at a more advanced stage; host tonalite shows moderately developed foliation. Coin is 2.3 cm in diameter. (c) Fractures not distinguishable from main fabric; alteration and deformation at advanced stages; host tonalite strongly foliated and showing banded fabrics. Microfabric of pale colored, banded domains is shown in Fig. 6(c). Pencil is *ca* 10 cm long.

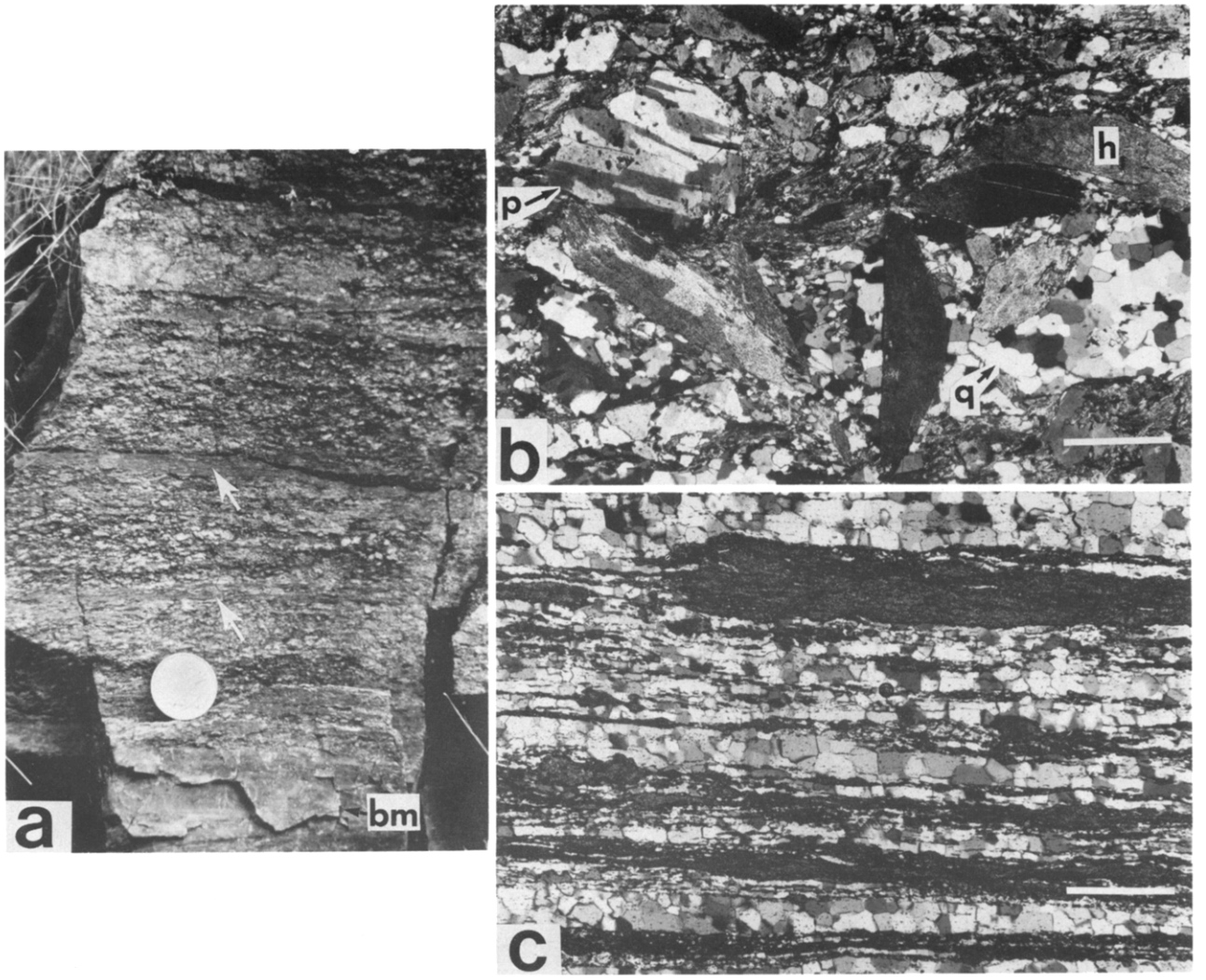

Fig. 5. Photographs of structures and fabrics in the Blackman's Creek tonalite (BCT), Lachlan Fold Belt, southeastern Australia. (a) Field photograph of banded mylonite in various stages of development. Thick band (**bm**) beneath coin and other thinner comparable bands (e.g. arrows) above coin appear as *banded mylonite* in thin-sections as shown in (c). Regions between vary from fabrics shown in (b) to those in (c). Coin is 2.8 cm in diameter. Specimen located 0.7 km northeast of Yarraman in fig. 3 of Tobisch & Paterson 1990. (b) Photomicrograph of 'least deformed' tonalite. Hornblende (**h**) is often twinned, and locally is rimmed with epidote and/or shows undulatory extinction. Plagioclase (**p**) shows complex deformation twins, with some crystals showing brittle behavior. Quartz (**q**) occurs in elongate aggregates of unstrained neoblasts. Bar scale is 0.4 mm. Viewed with crossed polarizers. Specimen located *ca* 3 km southeast of Yarraman, as above. (c) Photomicrograph of banded mylonite, consisting of bands of neoblastic quartz alternating with bands of granular very fine-grained epidote. Trace amounts of chlorite or actinolite may be present locally. Note tabular shaped quartz with planar crystal boundaries bordered by domains of epidote, textures comparable to that found in the SCMT banded mylonite (Fig. 6c). Bar scale 0.4 mm. Viewed with crossed polarizers. Locality same as in (a).

Fig. 6. Photomicrographs of structural features in the Santa Cruz Mountain tonalite (SCMT) and Blackman's Creek tonalite (BCT). (a)–(c) show progressive development of mylonitic fabric in the SCMT, and (d)–(f) show different features of epidote–quartz microveins in the two plutons. Samples cut parallel to stretching lineation. (d) & (f) (see p. 1144) viewed in plain light, all others with crossed polarizers. (a) Weakly to moderately developed foliation in SCMT inclined gently to left, and defined mostly by elongate aggregates of neoblastic quartz (**q**) and crudely aligned domains of primary (often twinned) hornblende (**h**). Minor epidote is selectively replacing plagioclase (**pe**), but the latter shows only slight deformation in thin-section. Bar scale is 2 mm. (b) Sample of SCMT showing moderately developed foliation, defined mostly by highly strained quartz aggregates and epidote–quartz microveins (especially in upper part of photograph). The microveins occur parallel or at some angle to the foliation. Epidote–quartz occur in areas more intensely deformed than contiguous regions. Note bent and faulted twins in plagioclase, and its selective replacement by epidote (**e**), including clot of massive granular epidote replacing fractured plagioclase (**p**) at right center. Bar scale is 0.4 mm. (c) Banded mylonite in SCMT, consisting of alternating domains where either quartz or epidote predominate. Some domains also bear minor to trace amounts of chlorite or actinolite. Tabular shaped quartz neoblasts with planar crystal boundaries are bordered by epidote domains as in samples of BCT (Fig. 5c). Bar scale is 0.4 mm.

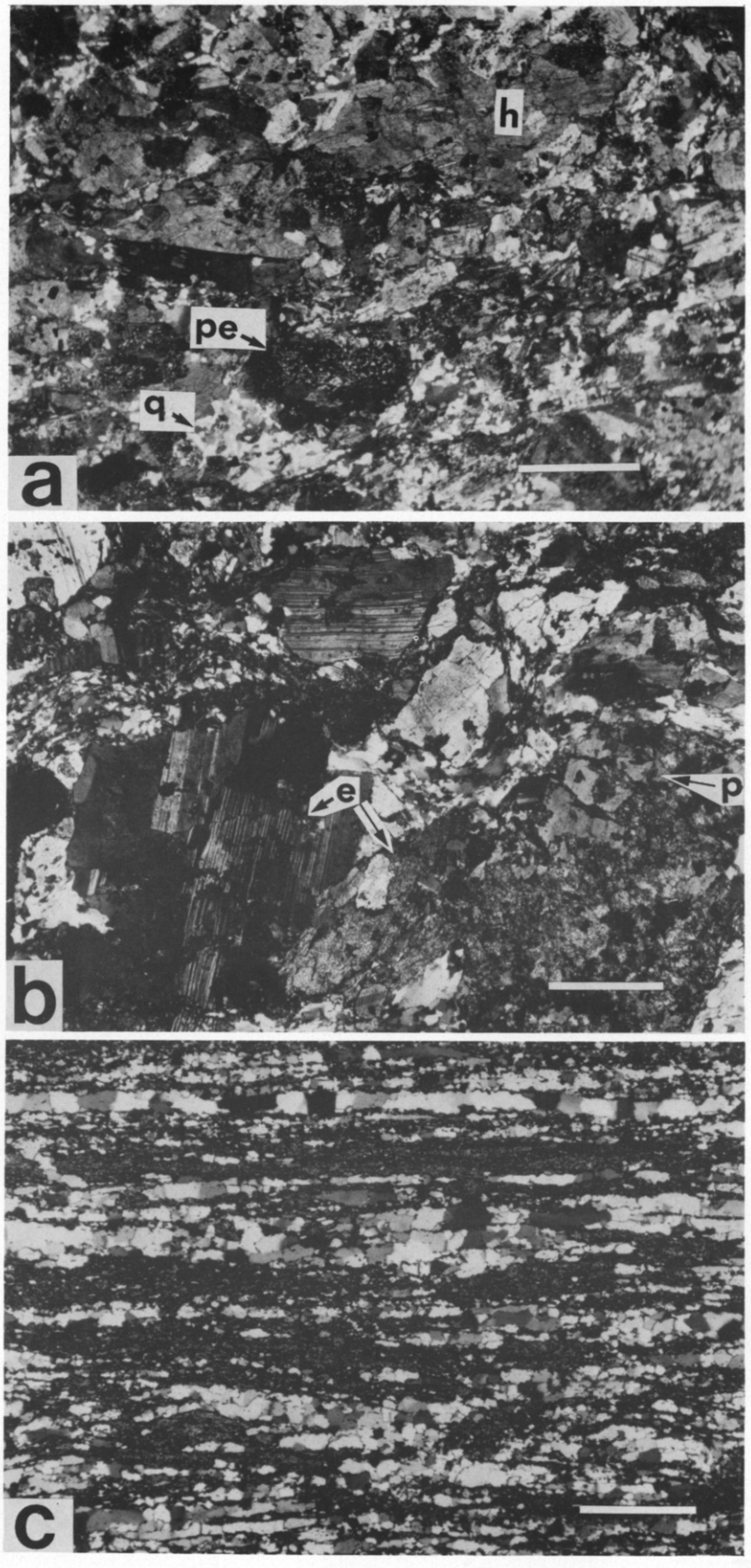

Fig. 6(a)–(c).

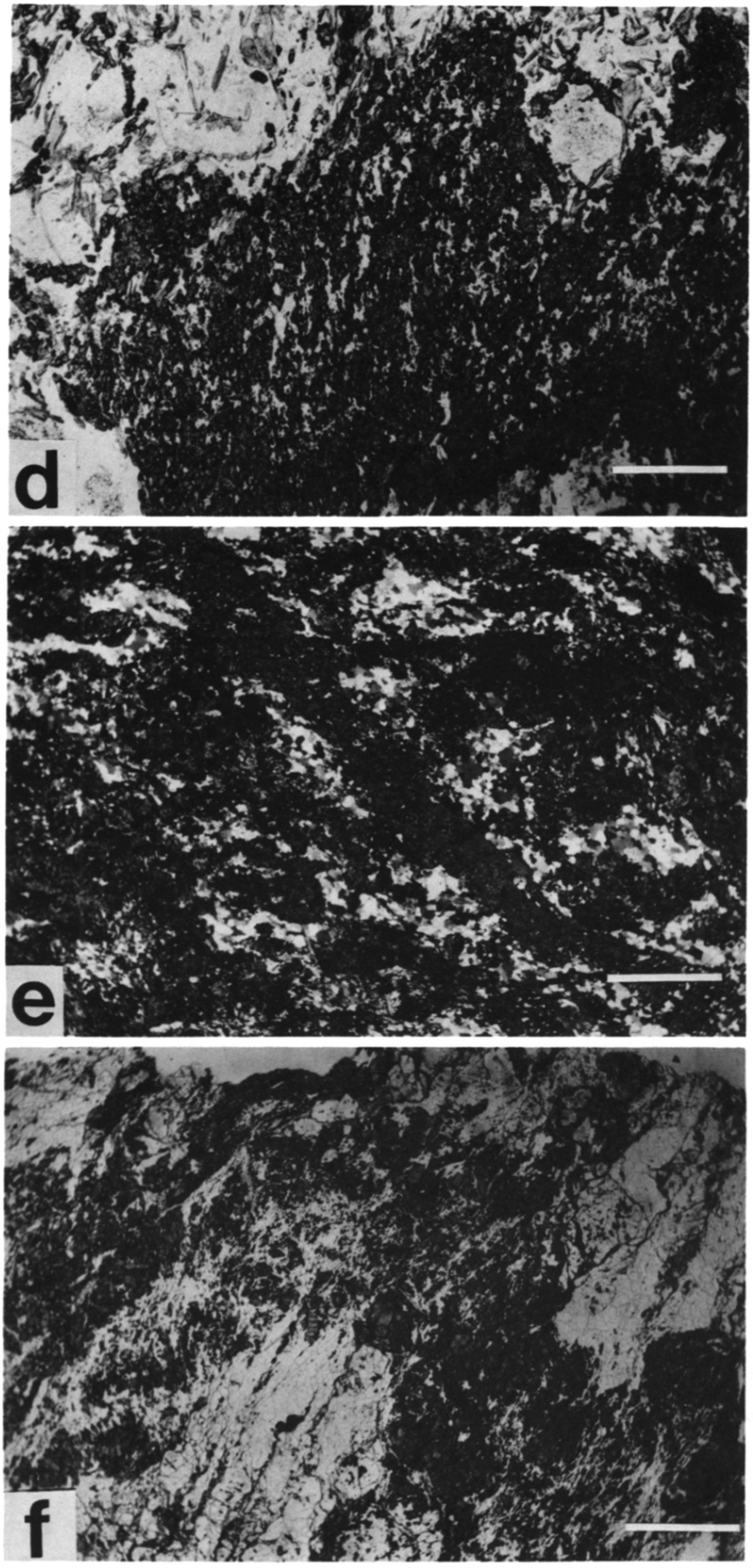

Fig. 6. (d) Microvein of granular and stringers of epidote neoblasts surrounding small elongate quartz neoblasts in SCMT, all aligned parallel to the predominant foliation in thin section (nearly vertically inclined in photo), suggesting epidote may have crystallized during deformation. Bar scale is 0.4 mm. (e) Microvein of granular fine-grained epidote inclined at *ca* 45° to right and cutting foliation at relatively high angle in SCMT. Foliation inclined more gently (*ca* 20°) to right, and is defined by elongate quartz masses and aligned chlorite. Epidote shows little evidence of deformation, suggesting this microvein may have formed late in, or after, the defomation at that point. Bar scale is 2 mm. (f) Folded epidote-rich microvein from sample of BCT. Axial plane foliation inclined steeply to left. Foliation morphology in microvein (e.g. lower right corner) and the high angle of foliation to the microvein suggests the microvein developed prior to or early in the deformation history at that point. Bar scale is 2 mm.

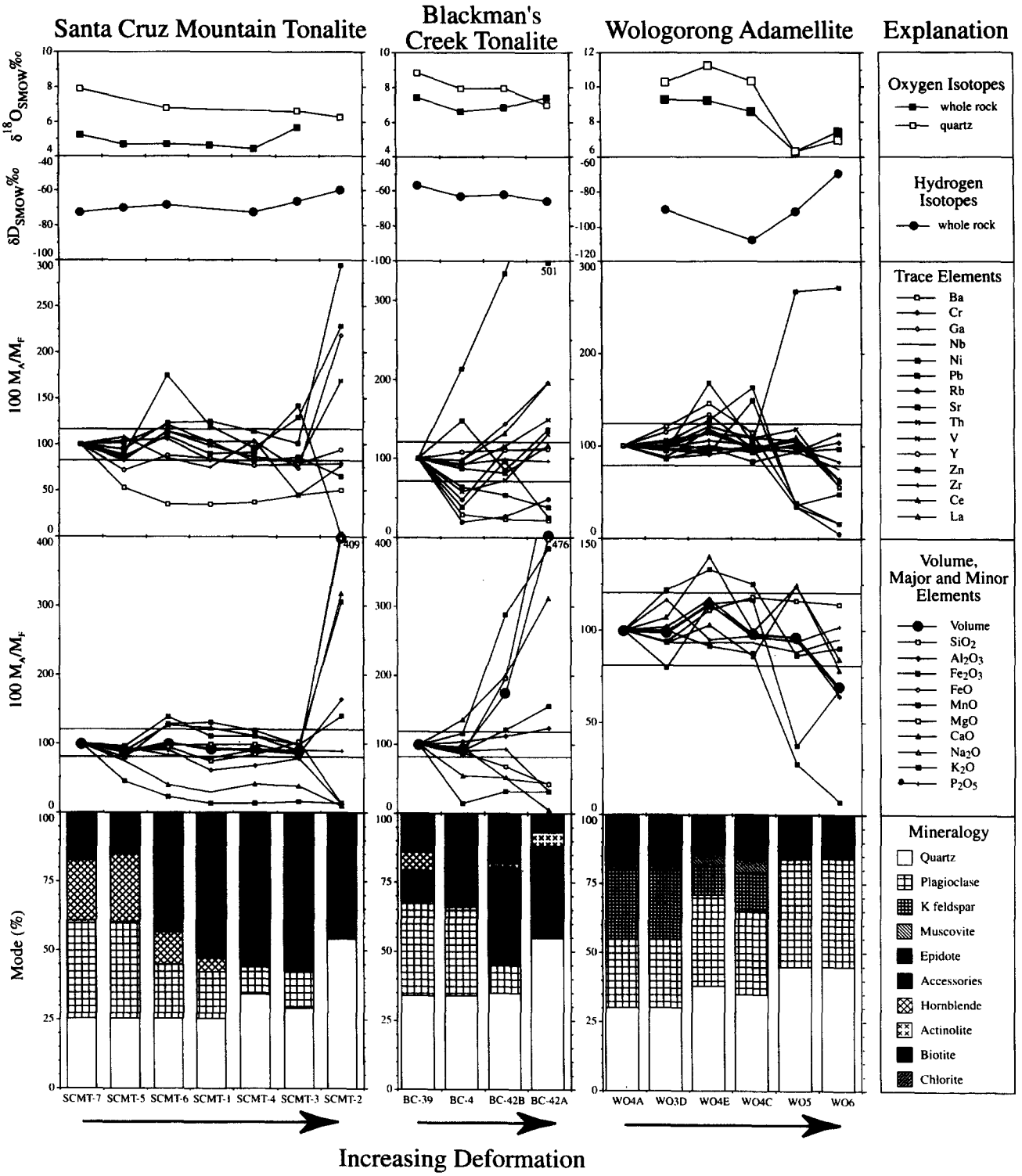

Fig. 7. Compositional changes plotted against increased fabric development (towards right) in the three suites. In SMCT, BCT and Wologorong suites, SCMT-2, BCT-42A represent the completed transition to banded mylonite and WO-5 and WO6 represent the partial (*ca* 50–60%) and total transition to ultramylonite, respectively. All samples normalized assuming conservation of TiO_2 (from data in Table 1). SCMT data normalized to SCMT-7, BCT data normalized to sample BC-39, and Wologorong granite data normalized to sample WO4A. Graphs show changes in: (i) modal mineralogy; (ii) major elements; (iii) trace elements; (iv) hydrogen isotopic composition of mafic concentrates; and (v) oxygen isotopic compositions of quartz separates and whole rock powders. The shaded bands in (ii) and (iii) indicate general ranges of minimal addition or subtraction (i.e. ±20%). See text for details.

quartz–epidote. Bands of essentially pure quartz or pure epidote also occur over limited regions. Banded mylonites from the SCMT and the BCT are nearly identical in gross morphology and mineralogy (cf. Fig. 4c with 5a, and 5c with 6c), although quartz grain boundaries in BCT samples exhibit substantially less undulatory extinction than banded mylonites from the SCMT;

(b) *non-banded quartz–epidote rocks* occur in many exposures in the SCMT and less commonly in the BCT. They are closely associated with the banded mylonites, and show a wide variety of textures, from strongly foliated to nearly isotopic. In places, uneven distribution of quartz and epidote produce a patchy texture, which may or may not be foliated. Undulatory extinction in both quartz and epidote vary from strong to absent, in some instances even within a thin-section.

In spite of the above variability, at least some domains show the following mineral changes with increasing recrystallization and fabric development (a–f; note: chlorite/biotite refers to mineral present in the SCMT/BCT, respectively):

(a) hble–plag–qtz (± epidote and chlorite/biotite)
(b) hble–plag–qtz–epidote–chlorite/biotite
(c) qtz–epidote–plag–chlorite/biotite (± hornblende)
(d) qtz–epidote–chlorite/biotite (± actinolitic amphibole)
(e) qtz–epidote (± chlorite/biotite and actinolitic amphibole)
(f) qtz–epidote.

The assemblages shown in the advanced stages of mylonitization (e and f) suggest metamorphic conditions of middle greenschist facies prevailed during mylonitization. The brittle deformation of igneous plagioclase, its lack of recrystallization and apparent removal by dissolution, plus the presence of plastic deformation mechanisms in quartz suggests temperatures during mylonitization were in the range 300–450°C (Voll 1976, Tullis 1983).

Microveins and their relation to mylonite genesis

Quartz–epidote assemblages are common along microfractures in the mylonite zones. The orientation of these microveins varies from inclined at a moderate angle to essentially parallel to the foliation. In addition, the microveins show evidence of pre-, syn- and post-kinematic development in various domains. Epidote in the microveins varies from aggregates with a strong preferred dimensional orientation (Fig. 6d) through equant grains with undulatory extinction to microveins transecting the foliation, the epidote showing no effects of deformation or preferred orientation (Fig 6e). In one sample from the BCT, a microvein at high angles to the foliation is folded, and epidote–quartz aggregates are orientated parallel to the axial plane of the fold (Fig. 6f).

Biotite adamellite from the Wologorong Batholith

Vernon *et al.* (1983) have described in detail the genesis of mylonite in the Wologorong Batholith, which we summarize to facilitate the discussion on chemical changes during mylonitization.

Deformation of the adamellite produced *S* and *C* folia (Berthé *et al.* 1979), the angle between which progressively decreased with increasing strain. Grainsize reduction by recrystallization and/or neocrystallization occurred in all minerals during the deformation, but quartz attained a steady-state grainsize of about 0.15 mm. Microfracturing of feldspar was prominent in the earlier stages of deformation, but evidence of recrystallization–neocrystallization is abundant in the more strongly deformed rocks. Plagioclase was the strongest mineral, so that unrecrystallized relics with igneous zoning (An_{48}–An_4) persist in strongly deformed rocks. Marginal recrystallization of both plagioclase (An_6–An_{24}) and microcline–microperthite is common. K-feldspar shows replacement by myrmekite + muscovite, marginally and along internal fractures. The myrmekite aggregates have recrystallized to form very fine-grained (0.02 mm) granular aggregates that make up local parts of *S* and *C* folia. Biotite has neocrystallized to fine-grained aggregates of new biotite ± muscovite in both *S* and *C* folia, generally with sphene ± epidote.

CHEMISTRY OF THE GRANITOIDS AND THEIR MYLONITIZED EQUIVALENTS

We have obtained whole-rock major and trace element analyses, as well as oxygen and hydrogen isotopic analyses of the granitoids at various stages of mylonitization, in order to characterize the chemical changes and constrain possible mechanisms of fluid–rock interaction. Six of the seven samples analyzed from the SCMT were cut from one block (measuring *ca* 10 × 35 × 45 cm) which showed a nearly complete range in intensity of deformation. The seventh (least deformed) sample was taken from a block a few meters away. Of four samples analyzed from the BCT, two showing most intense deformation were about 20 cm from each other in the same exposure, and the other two less-deformed samples were taken from different exposures in nearby areas (see Tobisch & Paterson 1990, fig. 3, for a more detailed geologic setting). The Wologorong samples were taken along a 300 m stream section, where the Abercrombie River crosses the batholith (Wol, Fig. 3, inset). Analyzed samples varied in weight from *ca* 0.15 to 0.25 kg.

Whole-rock major and trace element analyses were carried out at Macquarie University on a Siemens SRS1 automated X-ray fluorescence spectrometer, following the procedures and corrections of Norrish & Chappell (1977). Analyses of FeO, CO_2 and H_2O were carried out by standard wet chemical procedures.

Isotopic methods

Oxygen and hydrogen isotopic compositions of whole-rock powders, quartz separates and mafic mineral concentrates were measured using standard extraction

and mass spectrometric techniques. Quartz separates were prepared by sizing crushed samples, treating them with dilute HBF_4 to remove most other minerals, and handpicking the remaining contaminants. Mafic minerals were concentrated using magnetic separation techniques, but the grain size in most samples precluded complete mineral separation. Oxygen was extracted by fluorination with ClF_3 and converted to CO_2 by reaction with hot graphite (Borthwick & Harmon 1982). Hydrogen was extracted by heating the mafic concentrates to >1200°C and using hot U to convert the released water to H_2 (Friedman 1953). Isotopic composition of CO_2 and H_2 were measured on a Finnegan-MAT 250 mass spectrometer against working standards calibrated against NBS-28 ($\delta^{18}O_{SMOW}$ = +9.65‰) and V–SMOW (for H_2).

Metasomatic and isotopic changes

With increasing mylonitization, each of the three suites shows systematic variations in chemical and isotopic composition as well as mode (Fig. 7). In order to calculate metasomatic changes, specific knowledge is required of the variation in at least one characteristic of the system (the mass of a chemical component or the volume) during metasomatism (e.g. Gresens 1967, Grant 1986).

The rocks lack reliable indicators of volume change; so a chemical component must be found. Ideally, more than one chemical component should be conserved, so that relative changes of several elements during metasomatism are constant. Two lines of evidence identify conserved components: inferred low solubility during the process and coherent enrichments or depletions. In this study, each suite is normalized to its least deformed member, conserving the same component:

$$Mi_A/Mi_F = Ci_A/Ci_F \cdot C_{con_F}/C_{con_A}, \quad (1)$$

where Mi_A, Mi_F and Ci_A, Ci_F, C_{con_A} and C_{con_F} are the masses and concentrations of components i and the conserved component (subscript 'con') in the reference rock (subscript F) and the altered rocks (subscript A). Similarly, the relative change in volume is given by:

$$V_A/V_F = \rho_F/\rho_A \cdot C_{con_A}/C_{con_F}, \quad (2)$$

where V_A, ρ_A and V_F, ρ_F are volumes and densities of the altered and fresh rocks. The initial mass or volume considered is arbitrary.

The results (Table 1, Fig. 7) show that if TiO_2 is conserved, other low mobility components (Al_2O_3, P_2O_5, Cr, Ni, V, Y and Zr) are also approximately conserved (generally within ±20%). Under many conditions, Al and the high-field strength elements (Ti, Zr, etc.) are relatively insoluble (e.g. Correns 1978, Pascal & Anderson 1989). Thus one might normalize to any of these other components. TiO_2 or Al_2O_3, however, make the most sense for normalization because of their higher and thus more uniform and accurately determined concentrations, and we have normalized the analyses to TiO_2. The scatter in the data can be attributed to a combination of sample heterogeneities, particularly for minor minerals, high relative uncertainties in concentrations for elements near detectibility limits, and local mobility of some components (e.g. P_2O_5 and Ni) in the most intensely altered rocks. Other groups of components sometimes behave coherently and could, arbitrarily, be taken as 'immobile' if no further consideration were given. For example, CaO, Fe_2O_3 and Sr maintain similar ratios in the tonalitic suites, but their behavior is best interpreted as due to their coherent addition given their relatively high solubilities and their concentration in the same mineral, epidote.

The tonalitic suites have similar large enrichments in SiO_2, CaO, Fe_2O_3, total Fe, and Sr, and strong depletions in Na_2O, K_2O, FeO, MgO, Ba and Rb (Fig. 7). These shifts are consistent with the mineralogical changes: loss of plagioclase (Na, Ba) + hornblende (Na, K, Fe^{2+}, Mg) biotite (K, Fe^{2+}, Mg, Ba, Rb) and increased quartz (Si) + epidote (Ca, Fe^{3+}, Sr). The quartz–epidote banded mylonites of the tonalite suites (SCMT-2, BC-42A) gained approximately three times their original mass (mostly SiO_2) during this process. This must have been accommodated by similar dilational changes in volume as the densities vary little (Table 1, Fig. 1), and may be thought of as synkinematic formation of a quartz–epidote vein with accompanying wall-rock alteration. Behavior of the immobile elements is reasonably coherent, although their compositional patterns tend to be scattered.

The changes in the Wologorong suite with increasing deformation differ from the tonalitic suites in that only Sr is strongly enriched, and K_2O, Ba, Pb and Rb are strongly depleted (Fig. 7). SiO_2 and Al_2O_3, among others, show moderate depletions relative to TiO_2 (*ca* 30%), whereas the mafic + plagioclase constituents (Mg, Fe, Ca, Na) change little. The major losses (including Si and Al) are consistent with the removal of mainly K-feldspar and the possibility of mechanical segregation (discussed below). Sr must be added from an external source and fixed in plagioclase ± epidote.

All suites show systematic decreases in $\delta^{18}O$ and convergence of whole-rock and quartz compositions with increasing deformation. The convergence of quartz and whole-rock $\delta^{18}O$ values probably reflects the increasing percentage of quartz in the rocks. Calculated water $\delta^{18}O_{SMOW}$ for the *most altered* for all three suites is *ca* +2 ± 2‰ (at 350 ± 50°C, a plausible temperature for the retrogressive metamorphism accompanying deformation; the $^{18}O/^{16}O$ fractionation from Matsuhisa *et al.* 1979). Waters equilibrated with the quartz from the less deformed rocks would be correspondingly heavier. However, the quartz from each sample may be isotopically heterogeneous, reflecting mixtures of an original metamorphic quartz with fully exchanged mylonitized material.

The hydrogen isotope compositions of mafic minerals also change systematically with deformation within each suite. Reliable interpretation of these data is hindered by the present uncertainties in hydrogen isotope fractionations (O'Neil 1986) and the mixture of hydrous

Table 1. Samples from SCMT, BCT and WO Suites showing modal mineralogy, stable isotope composition, major and trace element compositions and gains/losses. See text for details

Sample Number	SCMT-7	SCMT-5	SCMT-6	SCMT-1	SCMT-4	SCMT-3	SCMT-2	BC-39	BC-4	BC-42B	BC-42A	WO-4A	WO-3D	WO-4E	WO-4C	WO5	WO6
	least deformed						most deformed	least deformed			most deformed	least deformed					most deformed
Mineral modes (%)																	
Quartz	25.5	25.0	25.0	25.0	34.0	29.0	54.0	34.0	34.0	35.0	55.0	30.0	30.0	38.0	35.0	45.0	45.0
Plagioclase	35.0	35.0	19.5	17.0	10.0	13.0	0.0	34.0	32.0	10.0	0.0	25.0	25.0	33.0	30.0	39.0	39.0
K-feldspar												25.0	25.0	10.0	14.0	0.0	0.0
Biotite								12.0	2.0	15.0	5.5	15.0	15.0	10.0	5.0	5.0	4.0
Chlorite	6.0	5.0	8.0	13.0	14.0	20.0	2.0	2.0	17.0	3.0	1.0	0.1	0.0	1.0	5.0	5.0	8.0
Muscovite												2.0	2.0	5.0	5.0	0.0	0.0
Hornblende	22.0	25.0	12.0	5.0	1.0	0.0	0.0	7.0	0.0	0.0	0.0						
Actinolite	0.0	0.0	0.0	0.1	0.1	0.0	0.1	0.0	0.0	2.0	5.5	0.0	0.0	0.0	0.0	0.0	0.4
Epidote	10.0	9.0	34.5	39.0	39.0	36.0	44.0	11.0	15.0	35.0	33.0	1.0	1.0	2.0	5.0	5.0	3.0
Sphene	0.1	0.1	0.1	0.0	0.1	0.0	0.0										
Accessories	1.5	1.0	1.0	1.0	1.5	2.0	0.0					2.0	2.0	1.0	1.0	1.0	0.8
Density (g cm^{-3})	2.86	—	—	—	—	—	2.99	2.83	—	—	3.16	2.725	—	—	—	—	2.731
Stable isotope compositions																	
$\delta^{18}O$ w.r.	5.2	4.7	4.7	4.7	4.4	5.7	9.6	7.4	6.6	6.8	7.4		9.3	9.2	8.6	6.3	7.4
$\delta^{18}O$ Qz	7.9		6.8		5.7	6.6	6.3	8.9	7.9	8.0	7.0		10.3	11.3	10.4	6.3	7.0
δD w.r.	−73	−70	−68		−72	−66	−60	−56	−63	−62	−66		−90		−108	−91	−70
Major element compositions (weight %)																	
SiO_2	58.17	59.18	56.71	59.71	59.83	58.02	78.06	67.74	64.57	78.19	88.46	72.80	72.61	72.87	72.42	72.97	72.86
TiO_2	0.67	0.75	0.67	0.70	0.70	0.78	0.22	0.51	0.56	0.30	0.14	0.32	0.32	0.28	0.33	0.34	0.47
Al_2O_3	16.17	15.94	16.32	15.42	15.37	15.98	8.74	13.35	15.22	8.83	4.56	13.81	14.11	14.15	13.93	14.12	13.10
Fe_2O_3	3.54	3.15	4.53	4.81	4.41	4.04	3.55	1.65	2.10	2.79	1.74	0.73	0.89	0.85	0.94	0.66	0.97
FeO	4.14	4.19	3.75	2.67	2.95	3.79	0.16	3.23	3.40	0.96	0.39	2.09	1.95	1.71	2.01	1.97	2.93
MnO	0.13	0.14	0.18	0.15	0.15	0.15	0.06	0.07	0.07	0.05	0.03	0.05	0.04	0.05	0.06	0.02	0.05
MgO	3.73	3.67	3.55	2.90	3.25	4.45	0.14	2.66	2.57	1.06	0.31	0.65	0.61	0.63	0.79	0.80	1.09
CaO	7.74	7.72	9.80	9.89	8.91	8.03	8.07	4.13	6.19	4.85	3.53	2.77	2.59	2.5	2.45	3.66	3.20
Na_2O	3.25	2.74	1.28	0.99	1.42	1.44	0.10	3.69	2.20	1.13	0.06	2.71	2.9	3.32	2.78	3.57	3.35
K_2O	0.22	0.11	0.05	0.03	0.03	0.04	0.01	1.13	0.18	0.21	0.10	3.03	3.03	2.42	2.74	0.88	0.31
P_2O_5	0.17	0.18	0.14	0.14	0.16	0.18	0.05	0.11	0.11	0.06	0.01	0.06	0.07	0.05	0.06	0.06	0.09
H_2O^+	1.97	2.10	2.67	2.54	2.66	3.26	0.87	1.40	2.33	1.37	0.66	0.81	0.70	0.77	1.19	0.84	1.27
H_2O^-	0.13	0.10	0.09	0.10	0.09	0.08	0.14	0.10	0.14	0.14	0.08	0.06	0.05	0.05	0.13	0.06	0.07
CO_2	0.16	0.16	0.03	0.06	0.05	0.11	0.10	0.30	0.08	0.12	0.08	0.03	0.04	0.04	0.08	0.07	0.19
Total	100.2	100.1	99.77	100.1	99.98	100.4	100.3	100.1	99.72	100.1	100.2	99.92	99.91	99.69	99.91	100.00	99.95
Trace element compositions (ppm)																	
Ba	141	83	49	52	55	74	23	257	82	35	16	466	564	597	547	188	109
Cr	31	36	33	27	25	28	8	87	46	57	27	15	13	12	15	15	23
Cu	30	37	29	34	36	49	23	14	11	11	12	3	4	6	18	1	1
Ga	14	13	16	15	15	12	10	13	14	11	7	16	16	17	18	18	15
Nb	0	0	0	0	0	0	0	0	0	0	0	10	10	10	10	10	11
Ni	14	16	17	15	12	14	3	14	6	8	1	7	6	6	6	7	10
Pb	4	4	7	5	4	6	3	8	13	4	3	25	26	28	42	9	6
Rb	3	1	1	0	1	1	0	45	10	7	6	131	136	110	131	48	10

Sr	343	363	423	449	408	402	331	162	380	318	223	145	138	213	155	411	578
Th	0	0	1	0	0	1	0	14	9	6	5	16	17	16	18	20	13
U	1	1	1	1	1	2	1	3	2	2	2	3	2	2	3	2	3
V	196	184	223	202	176	185	109	112	112	76	46	48	46	40	49	48	80
Y	26	21	23	23	21	24	8	26	31	17	8	40	46	47	40	45	33
Zn	66	64	72	62	63	109	0	48	34	15	5	47	45	38	72	18	33
Zr	126	153	107	99	137	66	32	132	136	77	35	131	130	122	136	137	160
La								25	24	12	8	70	67	61	67	76	66
Ce								54	58	42	29	32	28	33	32	37	29
Pr								5	8	0	0	25	31	29	28	39	31
Nd								22	30	18	13	9	10	13	11	14	14
$100 \cdot V_A/V_F$*																	
	100	(89)	(100)	(96)	(96)	(86)	317	100	(91)	(170)	407	100	(100)	(114)	(97)	(94)	68
$100 \cdot M_A/M_F$ major elements																	
SiO_2	100	91	97	98	98	86	409	100	87	196	476	100	100	114	96	94	68
TiO_2	100	100	100	100	100	100	100	100	100	100	100	100	100	100	100	100	100
Al_2O_3	100	88	101	91	91	85	165	100	104	112	124	100	102	117	98	96	65
Fe_2O_3	100	79	128	130	119	98	305	100	116	287	384	100	122	133	125	86	90
FeO	100	90	91	62	68	79	12	100	96	51	44	100	93	94	93	89	95
MnO	100	96	138	110	110	99	141	100	91	121	156	100	80	114	116	38	68
MgO	100	88	95	74	83	102	11	100	88	68	42	100	94	111	118	116	114
CaO	100	89	127	122	110	89	318	100	136	200	311	100	94	103	86	124	79
Na_2O	100	75	39	29	42	38	9	100	54	52	6	100	107	140	99	124	84
K_2O	100	45	23	13	13	16	14	100	15	32	32	100	100	91	88	27	7
P_2O_5	100	95	82	79	90	91	90	100	91	93	33	100	117	95	97	94	102
H_2O^+	100	95	136	123	129	142	134	100	152	166	172	100	86	109	142	98	107
H_2O^-	100	69	69	74	66	53	328	100	128	238	291	100	83	95	210	94	79
CO_2	100	89	19	36	30	59	190	100	24	68	97	100	133	152	259	220	431
Total	100	89	100	96	96	86	305	100	91	170	365	100	100	114	97	94	68
$100 \cdot M_A/M_F$ trace elements																	
Ba	100	53	35	35	37	45	50	100	29	23	23	100	121	146	114	38	16
Cr	100	104	106	83	77	78	79	100	48	111	113	100	87	91	97	94	104
Cu	100	110	97	108	115	140	233	100	72	134	312	100	133	229	582	31	23
Ga	100	83	114	103	103	74	218	100	98	144	196	100	100	121	109	106	64
Nb												100	100	114	97	94	75
Ni	100	102	121	103	82	86	65	100	39	97	26	100	86	98	83	94	97
Pb	100	89	175	120	96	129	228	100	148	85	137	100	104	128	163	34	16
Rb	100	30	33	0	32	29	0	100	20	26	49	100	104	96	97	34	5
Sr	100	95	123	125	114	101	294	100	214	334	501	100	95	168	104	267	271
Th								100	59	73	130	100	106	114	109	118	55
U	100	89	100	96	96	172	305	100	61	113	243	100	67	76	97	63	68
V	100	84	114	99	86	81	169	100	91	115	150	100	96	95	99	94	113
Y	100	72	88	85	77	79	94	100	109	111	112	100	115	134	97	106	56
Zn	100	87	109	90	91	142	0	100	65	53	38	100	96	92	149	36	48
Zr	100	108	85	75	104	45	77	100	94	99	97	100	99	106	101	98	83
La								100	87	82	117	100	96	100	93	102	64
Ce								100	98	132	196	100	88	118	97	109	62
Pr								100	146	0	0	100	124	133	109	147	84
Nd								100	124	139	215	100	111	165	119	146	106

*Values in parentheses indicate the density in the volume.

minerals in each sample. Estimated water δD values for the suites are: Blackman's Creek tonalite $-20 \pm 20‰$; Santa Cruz Mountain tonalite $-20 \pm 20‰$, and Wologorong granite $-35 \pm 20‰$. The overall variation within each sample suite is roughly consistent with changes in bulk fractionation, reflecting the variations in abundances of the hydrous minerals. Although the several hydrous minerals in the samples may be of different generations they have all been at least partially recrystallized during the deformation, thus facilitating re-equilibration with deformation-related fluids.

Interpretation

Fluid–rock interaction. The petrographic and geochemical data indicate substantial mass transfer over the width of the shear zones in all three suites (usually *minimum* distances of tens of centimeters). Two mechanisms are possible: (1) small-scale (cm–m), mechanical and (or) diffusional segregation localized within the deformation zones, or (2) infiltration of chemically distinct fluids along the deformation zone from more distant sources.

The originally homogeneous composition of the tonalitic rocks (on scales greater than a few cm) makes it unlikely that simple mechanical segregation was the source of differences found in the banded mylonite. The compositional changes are generally monotonic and there is no evidence for complementary enrichments and depletions in the adjacent rocks within the zone of deformation. Similarly, the original mineralogical uniformity precludes local chemical potential gradients to drive diffusive segregation. The high-variance mineral assemblages in the most deformed rocks (e.g. SCMT-2) also indicate open-system behavior. Diffusion may have been important, but it would have been in response to chemical potentials externally imposed by infiltrating fluids.

The less distinct changes in the Wologorong suite (Fig. 7, Table 1) can be interpreted best as a combination of modest infiltration-driven mass transfer and local mechanical segregation. Even the most deformed rocks (WO5, WO6) have comparatively low-variance mineral assemblages. Only the potassium group of elements (K, Rb, Ba, Pb) is strongly depleted, requiring fluid infiltration. The crude complementarity in the enrichment of mafic components (Mg, Ti) vs depletion of felsic components (Si, Al, Na) indicates that some of the effect may be due simply to modal differences. Possibly, an original heterogeneous distribution of mafic minerals in the mafic-poor adamellite was enhanced by deformation. Of course, original heterogeneity in TiO_2 increases uncertainty in normalization; however, this affects mainly those elements that show small changes (e.g. MgO, CaO). Larger changes as seen in alkalis (K_2O, Rb, etc.) must be real and close to the amounts indicated. The lower total TiO_2 also contributes to the uncertainty in the normalization.

Infiltration of fluids over significant distances (probably $\gg$ 10 m) is required to account for the observed mass transfer of all elements in the three suites. The scale of transfer depends on the origin of the fluids. If fluids equilibrated with different rock-types, transport need not have been far (i.e. only the distance to the contact, >100 m in each suite). Material possibly could have been transported by diffusion between distinct rock-types (e.g. between carbonate and silicate rocks) over shorter distances at similar temperatures and pressures, however. The principal compositional changes in the tonalitic suites are not consistent with this diffusion. For example, silica is the main constituent added to the tonalites, yet the protoliths contain quartz. Thus, there would have been no drive to diffuse silica into them. The less extensive transfer in the Wologorong suite might be interpreted as due to infiltration of fluids from a local, lower pH, quartz-absent rock-type (e.g. a quartz-free pelitic rock; however, there is no evidence for appropriate rocks nearby, Vernon *et al.* 1983).

The likely cause of mass transfer is changes in mineral solubilities with pressure and temperature along the fluid flow path, perhaps coupled with compositionally distinct sources. Many paths can be constructed that would produce the observed changes. As a generalization, quartz precipitation and hydrolysis reactions (leaching of alkalis and alkaline earths) occur with decreasing temperature and/or pressure (Walther & Helgeson 1977, Meyer & Hemley 1967). The compositional changes observed are thus broadly consistent with influx of cooling, rising(?) fluids.

Qualitative estimates of the minimum amounts of fluid passing through these rocks can be made from the compositional changes. Rock δDs are most sensitive to fluid addition, because of the low hydrogen content of most rocks. As noted above, the rocks from each suite appear to have equilibrated their hydrogen isotopes with a common fluid. This implies a minimum water/rock ratio (weight basis) of *ca* 0.1, even in the least deformed materials. Oxygen isotope shifts require minimum water/rock ratio of *ca* 3–5 in the most intensely deformed rocks, namely the quartz–epidote and quartz–plagioclase mylonites. Substantially lower values are probable in the less deformed rocks of the same suites (water/rock <1 in the least deformed), but reliable estimates are precluded by the lack of initial igneous and pre-deformation metamorphic compositions for these suites.

Chemical changes can also be used to infer amounts of fluids. Changes in SiO_2 contents offer the best constraints, because silica solubility in aqueous fluids depends mainly on temperature and pressure. If total salinities were known, it would be possible to make analogous use of changes in the other major elements, which are complexed by chloride. However, the necessary evidence (from fluid inclusion data or Cl contents of hydrous silicates) is unavailable. For silica, solubilities at a few kb pressure and 300–400°C are a few g per kg of solution (Walther & Helgeson 1977). Thus, if the excess quartz (*ca* 3 g new quartz per 1 g original rock in the BCT and SCMT suites) formed by complete precipitation

from saturated fluids, local fluid/rock values would have been *ca* 10^3. Of course, complete precipitation is unreasonable; so the actual integrated flux would be substantially higher.

A more severe constraint arises for the Wologorong suite if Al_2O_3 is leached, as suggested by normalization to TiO_2 (Table 1). Aqueous Al_2O_3 concentrations for upper greenschist conditions for muscovite–quartz–K-feldspar assemblages are of the order of 0.01 g kg^{-1}, as extrapolated from the experimental results of Pascal & Anderson (1989), and thus require minimum water/rock of the order of 10^4 to explain the compositional changes. Alternatively, if the feldspathic component were locally segregated out of the most intensely deformed rocks (e.g. due to differential mechanical behavior), large amounts of fluid would be unnecessary. Similar large (local?) losses of Al_2O_3 are evident in the Fries fault zone, Virginia and North Carolina, as inferred from the data of O'Hara & Blackburn (1989). In both areas, approximate conservation of mafic components and relatively small changes in silica contents argue against exceptionally high (i.e. $>10^3$) fluid/rock ratios. Therefore, given (from the above reasoning) that extensive Al mobility appears unlikely, the K-leaching and water addition in the Wologorong suite can be consistent with fluid/rock ratios of as little as *ca* 10 (with moderately saline, mildly acid fluids).

Source of fluids. On the basis of our limited sample set, it is difficult to identify with certainty the sources of the fluids. The original SCMT rock oxygen isotopic compositions compare well with isotopic compositions of other Foothills belt granitoids (Masi *et al.* 1981); however, a magmatic source for fluids is unlikely. Calculated water hydrogen compositions are isotopically heavier than typical magmatic water hydrogen and the shift in rock oxygen is inconsistent with equilibration with water cooled from a magmatic-composition source (Taylor 1979). Metamorphic waters also seem unlikely: calculated water isotopic composition have considerably lighter oxygen and somewhat heavier hydrogen than most metamorphic waters (Taylor 1979). Waters with metamorphic O and H signatures in the early Cretaceous Mother Lode quartz veins of the western Sierra Nevada have similar to lighter δD (-30 ± 20‰), but much heavier $\delta^{18}O$ (11 ± 3‰), which is compatible with oxygen added from regional metasedimentary rocks (Böhlke & Kistler 1986). A single analysis of an undeformed quartz vein in the SCMT revealed similarly heavy oxygen ($\delta^{18}O$ of +13.8‰), much heavier than oxygen in quartz from the mylonite zones.

Calculated oxygen and hydrogen isotopic compositions from all three locations most closely resemble modified seawater or connate water. Extensive Jurassic hydrothermal alteration in the western Great Basin and Ritter Range pendant of the Sierra Nevada formed from fluids with similar isotopic compositions; those fluids have been interpreted as connate water or partly exchanged seawater (Battles & Barton 1989, Hanson *et al.* 1990).

DISCUSSION AND CONCLUSIONS

The field, petrographic and geochemical observations presented above demonstrate that substantial compositional changes occurred in the shear zones. However, questions remain about the temporal development of deformation and mass transfer, the genetic relationship between the two, and the broader significance of fluids and mass transfer during shearing in these three areas and in other shear zones. In the following section, we discuss some of the ambiguities in timing, compare our results with published studies in other shear zones, and conclude with a synopsis of possible mechanisms.

Temporal development of the tonalitic and adamellite suites

In the tonalite suites studied herein, large changes in ratios of major and trace elements suggest substantial movement of fluids and profound exchange between the fluids and the granitoid. However, textural evidence from different tonalite specimens does not readily discriminate among the various possibilities (Fig. 1), and few observations constrain timing of mass transfer in the shear zones thoughout the regions. This is a common dilemma in interpreting movement/fluid timing in shear zones (e.g. Rutter & Brodie 1985).

In some domains banded mylonites appear to have developed from the hornblende tonalite during progressive deformation and in the presence of fluids (Fig. 1c). These domains show a maximum change in chemical constituents. Although alkalis and alkaline earths may be mobilized from little deformed rocks (Fig. 7), the major gains (SiO_2, CaO and Fe_2O_3) and losses (K_2O, Na_2O, FeO and MgO) occur mostly in the highly strained rocks, providing striking examples of channelized fluid flow. We interpret the non-banded quartz–epidote rocks to represent recrystallization and neocrystallization taking place by interaction between fluids and the tonalite in zones where tectonic movement was substantially reduced or entirely absent. These may be places where fluids migrated out of active shear domains and reacted with earlier deformed tonalite under relatively static conditions. Variable superposition of these processes—static and dynamic recrystallization, with and without infiltration—probably produced the complex sequences implied in Fig. 1(e).

It has been suggested that deformation in the Foothills Terrane proceeded in a domainal and strongly diachronous fashion (Tobisch *et al.* 1989). At the earliest stages, hydraulic fracturing may have been important and formed the fracture sets along which the initial alteration took place (as suggested by Segall & Simpson 1986, for mylonite zones in a granitic pluton in the eastern Sierra Nevada). However, as the process continued, the role of fracturing gave way to solution, crystal-plastic and recrystallization processes, which predominated during development of the banded mylonites along which focussed fluid flow occurred. Much of the volume gain shown by the banded mylonites must have taken place at

these later stages (Fig. 7). We propose that the macro- and microtextural evidence and the mineralogical zoning are consistent with episodic movement and shifting of anastomosing mylonite domains in the tonalites. Such a movement pattern may have combined with cyclical influxes of fluids changing composition with time (e.g. Fe^{3+} and other compositional zoning in epidote and chlorite mentioned earlier), perhaps generated by dilatancy pumping (Sibson 1980, 1981, Gapais & White 1982, Passchier 1982, Knipe & Wintsch 1985, Reynolds & Lister, 1987, McCaig 1988, Nur & Walden 1989), and could explain the complex temporal–spatial relations between deformation and mass transfer.

The Wologorong adamellite suite has simpler characteristics compared to the tonalitic suites. Chemical exchange is subdued and there is little evidence for repetitive fluid introduction or the complex shifting of the locus of deformation and recrystallization. The microtextural data are much more consistent with development of a single period of shear activity accompanied by metamorphism, and its evolution is characterized by the lack of abundant fluids and their attendent chemical–mechanical effects.

Comparison with other shear zones

Deformed granitoids vary widely in chemical response to mylonitization (Table 2). Workers studying other mylonite zones have related maximum chemical change with zones of highest strain (Beach 1976, Marquer *et al.* 1985, Sinha *et al.* 1986, 1988, O'Hara 1988). However, the identity and amount of elements that are gained or lost vary considerably between areas (Table 3; where possible, our comparison is based on renormalization of published results).

We suggest that the variations (Tables 2 and 3) depend on several factors, including: (1) protolith composition; (2) mineralogy; (3) primary textures (e.g. grain-size distribution); (4) temperature; (5) pressure; (6) porosity changes; (7) strain rate; (8) tectonic environment; (9) fluid/rock ratio (fluid flux); (10) fluid source; and (11) fluid flow path.

Obviously, substantially different bulk compositions and mineral assemblages (factors 1 and 2) such as felsic and mafic gneisses (Winchester & Max 1984), show marked differences in chemical behavior during deformation. Smaller differences in protolith compositions should still influence relative gains and losses (compare the tonalitic (SCMT/BCT) with the granodiorite–quartz monzonite suites (WO), and published data on granitoid-hosted shear zones, Table 2). This is expected from the differences in fluid compositions equilibrated with the different primary and metamorphic mineral assemblages (e.g. Bowers *et al.* 1984). Primary textures (factor 3), especially grain-size distribution, could affect timing of component mobilization. For example, megacrysts of K-feldspar and/or plagioclase commonly are mechanically resistant during early stages of the deformation at greenschist facies conditions. They thus offer only a relatively small surface area for reaction with fluids (compared to feldspar in an equigranular and/or fine-grained granitoid). This surface-to-volume difference will affect the rate at which Na^+, K^+, Ca^{2+}, etc., go into solution (Walther & Wood 1984). For this reason, dissolution rates might be low during early stages of deformation of a coarse-grained rock, the overall duration of deformation ultimately influencing the degree to which those constituents are gained or lost. Factors (1)–(3) may partly explain the differences between the SCMT/BCT suites and the other suites, as the tonalites are more mafic and less porphyritic than the felsic granitoids.

The metamorphic conditions (factors 4–5) attending deformation are similar for many of the felsic examples. Though these two factors (4–5) cannot be neglected because they control equilibrium constants as well as influence rock rheology (deformation mechanisms), they probably have not played a large role in bringing about the observed chemical variations. For example, data in Table 3 demonstrate that even where primary

Table 2. Summary of changes observed in major elements from a selection of published data. Gained/lost implies >20% change. See text for details

Area	Host	Changes observed	Reference
SCMT and BCT	tonalite	Ca, Fe, Si, Sr gained Na, K, Mg, Rb lost	this study
WO	adamellite	Sr gained; K, Si, Al, Rb lost	this study
Bitterroot	granite	changes minimal	Kerrich & Hyndman (1986)
Picacho (lower)	granite	Fe gained	Kerrich & Rehrig (1987)
Pyrenees	diorite	K gained Ca lost	McCaig (1984)
Pyrenees	granite	K lost	McCaig (1984)
Brevard fault	granite/granodiorite	Ca, Fe gained K, Na, Si lost	Sinha *et al.* (1986)
Roffna granite (Switzerland)	granitoid	Na, Si, Sr lost Mg gained	Vocke *et al.* (1987)
Barrego Springs	granodiorite	K gained	Goodwin (1988)
Grimsel granite (Switzerland)	granodiorite	K, Mg gained Na, Ca lost	Marquer *et al.* (1985)
Rector Branch	granodiorite	K, Si, Al, Rb lost	O'Hara (1988)
Fries	granite	Na, K, Si, Al lost	O'Hara (1990)

Table 3. Comparison of major element chemistry, modal data, metamorphic facies, and gains/losses in undeformed and deformed suites of granitoids from six different shear zones. See text for discussion

	Undeformed samples						Most deformed samples						Gains/losses					
	WO	HEND	GRIM	RECT	SCMT	BCT	WO	HEND	GRIM	RECT	SCMT	BCT	WO	HEND	GRIM	RECT	SCMT	BCT
SiO_2	72.8	72.8	65.6	72.2	58.2	67.7	72.9	64.5	65.4	68.2	78.1	84.5	(0)	(−)	(0)	(−)	(+)	(+)
Al_2O_3	13.8	13.8	15.9	14.8	16.2	13.3	13.1	17.5	16.7	14.6	8.7	4.6	(+)	(+)	(+)	(0)	(−)	(−)
Fe_2O_3	0.7	—	TOT−	1.6	3.5	1.7	1.0	—	TOT−	3.7	3.5	1.7	TOT−	TOT−	TOT−	FE3−	TOT−	TOT−
FeO	2.1	2.0	4.2	—	4.1	3.2	2.9	2.9	3.8	—	0.2	0.4	(+)	(+)	(−)	(+)	(−)	(−)
MnO	0.05	0.04	0.08	0.02	0.1	0.07	0.05	0.2	0.06	0.04	0.06	0.03	(0)	(+)	(+)	(−)	(−)	(−)
MgO	0.7	0.5	1.1	0.3	3.7	2.7	1.1	0.4	2.6	0.9	0.1	0.3	(+)	(−)	(+)	(+)	(−)	(−)
CaO	2.7	1.2	3.0	1.2	7.7	4.1	3.2	3.2	0.7	2.7	8.1	3.5	(+)	(+)	(−)	(+)	(+)	(−)
Na_2O	2.7	3.1	4.5	3.4	3.2	3.7	3.4	2.4	3.1	3.6	0.2	0.06	(+)	(−)	(−)	(+)	(−)	(−)
K_2O	3.0	5.1	3.2	5.3	0.2	1.1	0.3	5.5	4.8	2.9	0.01	0.1	(−)	(+)	(+)	(−)	(−)	(−)
QZ	30	26	20	30	25	34	45	34	—	45	54	55						
PL	25	25	50	9	35	34	39	19	—	4	0	0						
KSP	25	25	15	40	0	0	0	1	0	11	0	0						
BIO	15	11	15	4	0	12	4	1	—	12	0	5						
MUS	2	7	0	14	0	0	0	27	—	22	0	0						
CHL	TR	0	0	0	6	2	8	0	—	0	2	1						
EPD	1	3	0	2	10	11	3	14	—	2	44	33						
HBL	0	TR	0	0	22	7	0	0	0	0	0	0						
ACT	0	0	0	0	0	0	1	0	0	0	TR	6						
Metamorphic facies							BIO GS	BIO GS	BIO GS	CHL GS	GS−EAM	BIO GS						

WO = Wologorong adamellite, SCMT = Santa Cruz Mountain tonalite, BCT = Blackman's Creek tonalite, all data in this report, HEND = Henderson quartz monzonitic gneiss (average of domains 1a, 2a, and 4a for undeformed and domain 9c in deformed sample, table 1 of Sinha *et al.* 1988), GRIM = Grimsel granodiorite (Marquer *et al.* 1985), RECT = Rector Branch granitoid, data taken from samples 20a (unmylonitized gneiss) and 22b (mylonite) listed in O'Hara & Blackburn 1989; see also O'Hara (1988). TOT − 4.2 (etc.) and TOT (+)/(−), refers to total iron content and gain/loss of total iron, respectively; — = phase present but not modally determined; BIO or CHL GS = biotite or chlorite zones (respectively) of greenschist facies; EAM = epidote amphibolite facies.

igneous features (factors 1–3) and physical conditions (factors 4–5) were similar (cf. e.g. Wologorong and Henderson gneisses), substantial differences still occur, indicating the importance of other factors.

During deformation, porosity probably changes (factor 6), which would influence intergrated fluid flux and thus water/rock. Paleostrain rates (factor 7) are difficult to constrain for the mylonite and ultramylonite zones. Based on recent data from the SCMT (Tobisch *et al.* 1989), strain rates calculated for the general region are approximately 10^{-14}, which is within the expected 'normal' range (White 1975, Pfiffner & Ramsay 1982, Paterson & Tobisch 1989). Data from other mylonite zones suggest strain rates probably fluctuate considerably during the life of a shear zone (Sibson 1980, Passchier 1982, Wintsch & Knipe 1983). Strain rates (to a total accumulated strain) would also control time inferred for fluid flow. However, these two factors (6 and 7) probably cannot account for the chemical differences, as they reflect different *types* of reaction, not just different *degrees* of reaction.

Tectonic environment (factor 8), including orientation of the shear zones and their movement (thrust-slip, strike-slip or normal-slip), whether shortening or extensional regimes, etc., could strongly affect fluid sources, pathways and fluxes. However, without careful synthesis of regional data the effects of tectonic setting are difficult to identify and separate from the following factors.

Variations in fluid fluxes, sources, and paths (factors 9–11) yield the most satisfying explanations. Differences in fluid fluxes (factor 9) rationalize the chemical differences within and between our suites and, by extension, some of the other suites (Tables 2 and 3). Large compositional (and volume) changes imply very high local fluid/rock ratios (e.g. in the ultramylonite zones of SCMT and BCT, Fig. 7). Fluid source and fluid flow path (factors 10 and 11) govern composition and also play important and interrelated roles in establishing which components were lost or gained. Transformation of the tonalites to quartz–epidote rocks and changes observed in other suites demand fluids out of equilibrium with the original assemblages (Fig. 7 and Table 3). The disequilibrium may originate from compositionally distinct sources or from the changes in mineral–fluid equilibrium constants along the P–T path of the fluid. Relatively small differences in pH, salinity, f_{O_2}, etc., affect the ability of the fluids to dissolve or deposit many components (e.g. Bowers *et al.* 1984). In detail, many different reactions are possible depending on source and path, suggesting a rationale for differences among the various suites. As noted earlier, our results for all three suites appear most consistent with cooling fluids, although they may have had different sources and possibly different fluxes. In other shear zones, fluids may have been warming, resulting in susbstantially different compositional changes (e.g. Sinha *et al.* 1986).

In conclusion, significant differences in element behavior shown by the various mylonite zones (discussed above and in Tables 2 and 3) could depend on any of the 11 parameters discussed, and may largely reflect local conditions. Some differences between data sets may depend on the normalizations used, although mineral and chemical variations shown by the mylonitized tonalites from the Sierra Nevada and southeastern Australia show substantial differences from more deformed felsic granitoids elsewhere. At a minimum, it appears reasonable to interpret these differences in terms of the primary composition, mineralogy, and texture of the protolith (factors 1–3), but most importantly of fluid interaction (factors 9–11) active during deformation. In most examples, it appears that compositional changes in mylonitic shear zones result from significant fluid flow, the details of which (path, source, conditions) control the nature of the changes. Shearing and mylonitization may localize this fluid flow, or may be influenced by it (for example, by selective formation of quartz, weakening the rock), or may be largely independent of it. Only through additional investigations of shear zones and their broader settings will the variations be explained.

Finally, it is interesting to speculate on the apparent variability of element mobility found in mylonite zones formed in host rocks of essentially the same composition and under similar metamorphic conditions (Table 3). At outcrop scales, these variations may reflect non-linear deterministic (chaotic) behavior, where slight variations in initial conditions (e.g. factors 3 and 9) might lead to disparate results (i.e. gross local differences in metasomatic changes and wide variations in the timing and amount of strain, cf. Fig. 1). This concept may be a fruitful line of investigation in the future when attempting to account for complex chemical–deformational systems as we have touched upon in this contribution.

Acknowledgements—We are grateful for support from NSF grants EAR 8607017 and INT 861152 (O. T. Tobisch and S. R. Paterson), a grant from ACS-PRF (M. D. Barton), ARC grant A38415716 (R. H. Vernon), and a faculty grant from the University of California, Santa Cruz (O. T. Tobisch). Dr S. Sorensen generously analyzed a sample of epidote by back-scatter electron imagery for us. Two of us (O. T. Tobisch and S. R. Paterson) wish to thank the faculty and staff at the School of Earth Sciences, Macquarie University, Sydney, for their hospitality, and especially Dr R. H. Flood for carrying out preliminary chemical analysis of some Australian samples, Comments by Kieren O'Hara and an anonymous reviewer aided considerably in improving the original manuscript. Kieren O'Hara suggested tectonic environment as one of the 11 factors possible.

REFERENCES

Battles, D. A. & Barton, M. D. 1989. Na–Ca hydrothermal alteration in the western Great Basin. *Eos* 70, 1382.

Beach, A. 1976. The interrelations of fluid transport, deformation, geochemistry and heat flow in early Proterozoic shear zones in the Lewisian complex. *Phil. Trans. R. Soc. Lond.* **A280**, 569–604.

Berthé, D., Choukroune, P. & Jegouzo, P. 1979. Orthogneiss, mylonite and non-coaxial deformation of granites: the example of the South Armorican Shear Zone. *J. Struct. Geol.* **1**, 31–42.

Böhlke, J. K. & Kistler, R. W. 1986. Rb–Sr, K–Ar, and stable isotope evidence for the ages and sources of fluid components of gold-bearing quartz veins in the northern Sierra Nevada Foothills metamorphic belt, California. *Econ. Geol.* **18**, 296–322.

Borthwick, J. & Harmon, R. S. 1982. A note regarding ClF_3 as an alternative to BrF_5 for oxygen isotope analysis. *Geochim. cosmochim. Acta* **46**, 1665–1668.

Bowers, T. S., Jackson, K. J. & Helgeson, H. C. 1984. *Equilibrium Activity Diagrams for Coexisting Minerals and Aqueous Solutions at Pressures and Temperatures to 5 kb and 600°C*. Springer, New York.

Burg, J.-P. & Laurent, Ph. 1977. Strain analysis of a shear zone in a granodiorite. *Tectonophysics* **47**, 15–42.

Cas, R. A. F. 1983. Paleogeographic and tectonic development of the Lachlan Fold Belt, southern Australia. *Spec. Publ. geol. Soc. Aust.* **10**.

Chappell, B. W., White, A. J. R. & Hine, R. 1988. Granite provinces and basement terranes in the Lachlan Fold Belt, southeastern Australia. *Aust. J. Earth Sci.* **35**, 505–522.

Clark, L. D. 1964. Stratigraphy and structure of part of the western Sierra Nevada metamorphic belt, California. *Prof. Pap. U.S. geol, Surv.* **410**.

Choukroune, P. & Gapais, D. 1983. Strain pattern in the Aar granite (Central Alps): orothogneiss developed by bulk inhomogeneous flattening. *J. Struct. Geol.* **5**, 411–418.

Correns, C. W. 1978. Titantium. In: *Handbook of Geochemistry* (edited by Wedepohl, K. H.), Chap. 22. Springer, New York, 11–2.

Dipple, G. M., Wintsch, R. P. & Andrews, M. S. 1990. Identification of the scales of differential element mobility in a ductile fault zone. *J. metamorph. Geol.* **8**, 645–661.

Etheridge, M. A., Wall, V. J., Cox, S. F. & Vernon, R. H. 1984. High fluid pressures during regional metamorphism and deformation: implications for mass transport and deformation mechanisms. *J. geophys. Res.* **89**, 4344–4358.

Etheridge, M. A., Wall, V. J. & Vernon, R. H. 1983. The role of the fluid phase during regional metamorphism and deformation. *J. metamorph. Geol.* **1**, 205–226.

Ferry, J. M. 1986. Reaction progress: a monitor of fluid–rock interaction during metamorphic and hydrothermal events. In: *Fluid–Rock Interactions During Metamorphism* (edited by Walther, J. V. & Wood, B. J.). Springer, New York, 60–88.

Friedman, I. 1953. Deuterium content of natural waters and other substances. *Geochim. cosmochim. Acta* **4**, 89–103.

Fyfe, W. S., Price, N. J. & Thompson, A. B. 1978. *Fluids in the Earth's Crust*. Elsevier, Amsterdam.

Gapais, D. & White, S. H. 1982. Ductile shear bands in a naturally deformed quartzite. *Textures Microstruct.* **5**, 1–17.

Gibson, B. G. 1973. The geology of the Bigga–Tuena area, New South Wales. Unpublished B.Sc. thesis, Canberra, Australian National Univeristy.

Goodwin, L. B. 1988. Structural studies of two strongly deformed terranes in California and Arizona. Unpublished Ph.D thesis, University of California, Berkeley.

Grant, J. A. 1986. The isocon diagram—a simple solution to Gresens' equation for metasomatic alteration. *Econ. Geol.* **18**, 1976–1982.

Gresens, R. 1967. Composition–volume relationships of metasomatism. *Chem. Geol.* **2**, 47–55.

Hanmer, S. 1987. Textural map units in quartzo-feldspathic mylonitic rocks. *Can. J. Earth Sci.* **24**, 2065–2073.

Hanson, R. B., Sorensen, S. S., Barton, M. D. & Fiske, R. S. 1990. Long-term evolution of fluid flow in arcs: evidence from the Ritter Range Pendant, CA. *Geol. Soc. Am. Abs. w. Prog.* **22**, A211.

Hobbs, B. E. 1965. Structural analysis of the rocks between the Wyangala batholith and the Copperhania thrust, New South Wales. *J. geol. Soc. Aust.* **12**, 1–24.

Kerrich, R., Allison, I., Barnett, R. L., Moss, S. & Starkey, J. 1980. Microstructural and chemical transformations accompanying deformation of granite in a shear zone at Mieville, Switzerland: With implications for stress corrosion cracking and superplastic flow. *Contr. Miner. Petrol.* **73**, 221–242.

Kerrich, R. & Hyndman, D. 1986. Thermal and fluid regimes in the Bitterroot lobe–Sapphire block detachment zone, Montana: Evidence from $^{18}O/^{16}O$ and geologic relations. *Bull. geol. Soc. Am.* **97**, 147–155.

Kerrich, R. & Rehrig, W. 1987. Fluid motion associated with Tertiary mylonitization and detachment faulting: $^{18}O/^{16}O$ evidence from the Picacho metamorphic core complex, Arizona. *Geology* **15**, 58–62.

Knipe, R. J. & Wintsch, R. P. 1985. Heterogeneous deformation, foliation development, and metamorphic processes in a polyphase mylonite. In: *Metamorphic Reactions* (edited by Thompson, A. B. & Rubie, D. C.). Springer, New York, 180–210.

Marquer, D., Gapais, D. & Capdevila, R. 1985. Comportement chimique et orthogneissification d'une granodiorite en facies schistes verts (Massif de l'Aar, Alpes Centrales). *Bull. Mineral.* **108**, 209–221.

Masi, U., O'Neil, J. R. & Kistler, R. W. 1981. Stable isotope systematics of Mesozopic granites of central and northern California and southwestern Oregon. *Contr. Miner. Petrol.* **76**, 116–126.

Matsuhisa, Y., Goldsmith, J. R. & Clayton, R. N. 1979. Oxygen isotope fractionation in the system quartz–albite–anorthite–water. *Geochim. cosmochim. Acta* **43**, 1131–1140.

McCaig, A. M. 1984. Fluid–rock interaction in some shear zones from the Pyrenees. *J. metamorph. Geol.* **2**, 129–141.

McCaig, A. M. 1988. Deep fluid circulation in fault zones. *Geology* **16**, 867–870.

Meyer, C. & Hemley, J. J. 1967. Wall-rock alteration. In: *Geochemistry of Hydrothermal Ore Deposits* (edited by Barnes, H. L.). Holt, Rinehart, and Winston, New York, 166–235.

Mitra, G. 1978. Ductile deformation zones and mylonites: the mechanical processes involved in the deformation of crystalline basement rocks. *Am. J. Sci.* **278**, 1057–1084.

Miyashiro, A. 1973. *Metamorphism and Metamorphic Belts*. John Wiley and Sons, New York.

Norrish, K. & Chappell, B. W. 1977. X-ray fluorescence spectrometry. In: *Physical Methods in Determinitive Mineralogy* (edited by Zussman, J.). Academic Press, London, 201–272.

Nur, A. & Walden, J. 1990. Time dependent hydraulics of the Earth's crust. In: *The Role of Fluids in Crustal Processes*. National Academy Press, Washington, DC.

O'Hara, K. 1988. Fluid flow and volume loss during mylonitization—an origin for phyllonite in an overthrust setting. North Carolina, U.S.A. *Tectonophysics* **156**, 21–36.

O'Hara, K. 1990. State of strain in mylonites from the western Blue Ridge province, southern Appalachians: the role of volume loss. *J. Struct. Geol.* **12**, 419–430.

O'Hara, K. & Blackburn, W. H. 1989. Volume-loss model for trace element enrichments in mylonites. *Geology* **17**, 524–527.

O'Neil, J. R. 1986. Theoretical and experimental aspects of isotopic fractionation. In: *Stable Isotopes in High Temperature Geological Processes* (edited by Vålley, J. W., Taylor, H. P. & O'Neil, J. R.). *Rev. Mineral.* **16**, 1–40.

Pascal, M. L. & Anderson, G. M. 1989. Speciation of Al, Si, and K in supercritical solutions: Experimental study and interpretation. *Geochim. cosmochim, Acta* **53**, 1843–1855.

Passchier, C. W. 1982. Pseudotachylite and the development of ultramylonite bands in the Saint-Barthelemy Massif, French Pyrenees. *J. Struct. Geol.* **2**, 69–80.

Passchier, C. W. & Simpson, C. 1986. Porphyroclast systems as kinematic indicators. *J. Struct. Geol.* **8**, 831–843.

Paterson, S. R. & Tobisch, O. T. 1989. Rates of pluton emplacement and regional deformation: their influence on evaluating timing relationships. *Geol. Soc. Am. Abs. w. Prog.* **21**, A305.

Paterson, S. R., Tobisch, O. T. & Radloff, J. 1987. Post-Nevadan deformation along the Bear Mountains fault zone: implications for the Foothills Terrane, central Sierra Nevada, California. *Geology* **15**, 513–516.

Paterson, S. R., Tobisch, O. T. & Morand, V. 1990. The influence of large ductile shear zones on the emplacement and deformation of the Wyangala Batholith, SE Australia. *J. Struct. Geol.* **112**, 639–650.

Paterson, S. R., Vernon, R. H. & Tobisch, O. T. 1989. A review of criteria for determining magmatic and solid-state foliations in granitoids. *J. Struct. Geol.* **11**, 349–363.

Pfiffner, O. A. & Ramsay, J. G. 1982. Constraints on geological strain rates: arguments from finite strain states of naturally deformed rocks. *J. geophys. Res.* **87**, 311–321.

Ramsay, J. G. & Graham, R. H., 1970. Strain variations in shear belts. *Can. J. Earth Sci.* **7**, 786–813.

Reynolds, S. J. & Lister, G. S. 1987. Structural aspects of fluid-rock interaction in detachment zones. *Geology* **15**, 362–366.

Robinson, P., Spear, F. S., Schumacher, J. C., Laird, J., Klein, C., Evans, B. W. & Doolan, B. L. 1982. Phase relations of metamorphic amphiboles: Natural occurrence and theory. *Rev. Mineral.* **9B**, 1–228.

Rutter, E. H. & Brodie, K. H. 1985. The permeation of water into hydrated shear zones. In: *Metamorphic Reactions* (edited by Thompson, A. B. & Brodie, D. C.). Springer, New York, 242–250.

Segall, P. & Simpson, C. 1986. Nucleation of ductile shear zones on dilatant fractures. *Geology* **14**, 56–59.

Sibson, R. H. 1980. Transient discontinuities in ductile shear zones. *J. Struct. Geol.* **2**, 165–171.

Sibson, R. H. 1981. Controls on low-stress hydrofracture dilatancy in thrust, wrench and normal fault terrains. *Nature* **289**, 655–667.

Simpson, C. 1986. Fabric development in brittle-to-ductile shear zones. *Pure & Appl. Geophys.* **124**, 269–288.

Sinha, A. K., Hewitt, D. A. & Rimstidt, J. D. 1986. Fluid interaction and element mobility in the development of ultramylonites. *Geology* **14**, 883–886.

Sinha, A. K., Hewitt, D. A. & Rimstidt, J. D. 1988. Metamorphic petrology and strontium isotope geochemistry associated with the development of mylonites: an example from the Brevard fault zone, North Carolina. *Am. J. Sci.* **288A**, 115–147.

Taylor, H. P., Jr. 1979. Oxygen and hydrogen isotope relationships in hydrothermal mineral deposits. In: *Geochemistry of Hydrothermal Ore Deposits* (2nd edn) (edited by Barnes, H. L.). John Wiley and Sons, New York, 236–277.

Tobisch, O. T. & Paterson, S. R. 1990. The Yarra Granite: an intradeformational thrust-related pluton in the Lachlan Fold Belt, southeastern Australia. *Bull. geol. Soc. Am.* **102**, 693–703.

Tobisch, O. T., Paterson, S. R., Saleeby, J. B. & Geary, E. E. 1989. Nature and timing of deformation in the Foothills Terrane, central Sierra Nevada, California: its bearing on orogenesis. *Bull. geol. Soc. Am.* **101**, 401–413.

Tullis, J. 1983. Deformation in feldspars. In: *Feldspar Mineralogy, Volume* 2 (edited by Ribbe, H. P.). Miner. Soc. Am., 297–323.

Tullis, J. & Yund, R. A. 1985. Dynamic recrystallization of feldspar: a mechanism for ductile shear zone formation. *Geology* **13**, 238–41.

Tullis, J. & Yund, R. A. 1987. Transition for cataclastic flow to dislocation creep of feldspar: Mechanisms and microstructures. *Geology* **15**, 606–609.

Vernon, R. H., Paterson, S. R. & Geary, E. E. 1989. Evidence for syntectonic intrusion of plutons in the Bear Mountains Fault Zone, California. *Geology* **17**, 723–726.

Vernon, R. H., Williams, V. A. & D'Arcy, W. F. 1983. Grain-size reduction and foliation development in a deformed granitoid batholith. *Tectonophysics* **92**, 123–145.

Vocke, R. D., Jr., Hanson, G. N. & Grunefelder, M. 1987. Rare earth element mobility in Roffna Gneiss, Switzerland. *Contr. Miner. Petrol.* **95**, 145–154.

Voll, G. 1976. Recrystallization of quartz, biotite and feldspar from the Erstfeld to the Leventina nappe, Swiss Alps, and its geological significance. *Schweiz. miner. petrogr. Mitt.* **56**, 641–647.

Walther, J. V. & Helgeson, H. C. 1977. Calculation of the thermodynamic properties of aqueous silica and the solubility of quartz and its polymorphs at high pressures and temperatures. *Am. J. Sci.* **227**, 1315–1351.

Walther, J. V. & Wood, B. 1984. Rate and mechanism in prograde metamorphism. *Contr. Miner. Petrol.* **88**, 246–259.

White, A. J. R. 1983. Granitoid types and their distribution in the Lachlan Fold Belt, southeastern Australia. In: *CircumPacific Plutonic Terranes* (edited by Roddick, J. A.). *Mem. geol. Soc. Am.* **159**, 21–34.

White, S. 1975. Estimation of strain rates from microstructures. *J. geol. Soc. Lond.* **131**, 577–584.

Winchester, J. A. & Max, M. D. 1984. Element mobility associated with synmetamorphic shear zones near Scotchport, NW Mayo, Ireland. *J. metamorph. Geol.* **2**, 1–11.

Wintsch, R. P. & Knipe, R. J. 1983. Growth of a zoned plagioclase porphyroblast in a mylonite. *Geology* **11**, 360–363.